室蘭工業大学
学術資源アーカイブ
Muroran Institute of Technology Academic Resources Archive

ハノイ市における繊維質材料混合流動化処理土の埋戻し地盤への適用に関する研究

メタデータ	言語: eng 出版者: 公開日: 2015-12-22 キーワード (Ja): キーワード (En): 作成者: ズゥオン, クゥン フン メールアドレス: 所属:
URL	https://doi.org/10.15118/00005132

Chapter 6

Study on Establishment of a Procedure for Prediction of Train-induced Vibration from Tunnel in Vietnam

6.1 INTRODUCTION

By 2020, Hanoi will boast of fully operational, efficient high-speed metro rail. Two of the six metro lines covering over 100 km are under construction in Vietnam's capital and the country's second largest city. The project will increase the share of public transport, reduce congestion, and bolster local economic growth in the city. According to plans, the network should expand to over 170 km by 2030. As operation of the metro system, moving trains may generate ground vibrations which cause undesirable environment and economical impacts such as nuisance of the passenger along the rail and deterioration of the alongside existing building structures. However, up to now a prediction procedure of train-induced vibration from tunnel in conformity with condition of Vietnam has been not found in official standards or literatures, and then, the ground-borne vibration level are not estimated in environmental impact assessment.

For this purpose, this chapter describes establishment of a prediction method for ground-borne vibration from railway tunnels in conformity with condition of Vietnam. Two cases of shield tunnel shape and ground profiles, which are typical ones of Hanoi metro line No.3 currently under construction, were selected to analyze for this study. Train-induced dynamic loading on tunnel floor was simulated by means of a train-track-tunnel interaction model. Results of the simulation in term of force time history was input data for tunnel-soil interaction problem. The vibration propagation from the tunnel into the ground surface was analyzed by the 2-dimensional finite element method (FEM). Numerical results from the model in term of vibration velocity

allow estimating the vibration velocity level, and then it is applicable to the prediction of train-induced vibration propagated from railway tunnel.

6.1.1 Definition of vibration level

Vibration level is estimated from three parameters as displacement, velocity and acceleration. In Vietnam, vibration velocity is used to estimate the vibration level as an application standard. The abbreviation "VdB" is used for vibration decibels to reduce the potential for confusion with sound decibels (FTA, 2006). Accordingly, maximum vibration level is computed as following (SP, 2004):

$$\mathrm{L} = \max(L_i) \leq [\mathrm{L}] \ [\mathrm{VdB}] \tag{6.1}$$

Where:

$$\mathrm{L_i} = 20\log_{10}\frac{\mathrm{v_i}}{\mathrm{v_{ref}}}[\mathrm{VdB}] \tag{6.2}$$

$$v_i = \sqrt{\frac{1}{(t_2-t_1)f_{SP}}\sum_n v_n^2}\ [\mathrm{m/s}] \tag{6.3}$$

$$v_n = \sqrt{v_{xn}^2 + v_{yn}^2}\ [\mathrm{m/s}] \tag{6.4}$$

L: Maximum vibration level

L_i: Vibration level with time at time interval of ith one-second

[L]: Criteria for acceptable level of vibration

v_i: Root mean square vibration velocity of measurement point at ith one-second

v_{ref}: Reference vibration velocity, $v_{ref} = 5.10^{-8}$m/s (SP, 2004)

$t_2 - t_1 = 1\mathrm{s}$ (FTA, 2006; SP, 2004; Kurbatskii, 2008)

f_{SP}: Number of measured velocity data within one-second period

v_{xn}, v_{yn}, v_n : n^{th} Horizontal, vertical, and total vibration velocity at measurement point

According to Russia standard being used in Vietnam at present, the vibration prediction for building is assessed from the value of velocity at top of foundation (SP, 2004). Therefore, this chapter uses the velocity value at the ground surface to predict the vibration.

National Technical Regulation on Vibration has been promulgated by Natural Resources and Environment in 2010 (QCVN 27, 2010). The regulation gives criteria for acceptable levels of ground-borne vibration from any source such as trains, buses on rough roads, and constructions activities, blasting, pile-driving and operating heavy earth-moving equipment for residence. The maximum permissible level of vibration is assigned to be 75VdB. The value is also found in reports of Japan. The results of the Japanese study confirm the conclusion that at a vibration velocity level of 75 to 80 VdB, many people will find the vibration annoying (Tokita, 1975).

6.1.2 Problem of Tunnel-Soil interaction

To solve the tunnel-soil interaction problem under dynamic loading on tunnel, a structure-medium system with 2-D plane strain state is considered to analyze. The train

track system receives the moving load of train, and then transfers it to tunnel floor. This causes the seismic wave propagating in the medium and then affect nearby buildings and resident.

A finite domain from half-space system including structure and surrounding medium is considered to analyze. In principal, shape of the domain may be arbitrary. However, to simplify the analytical model, it is assumed to be rectangle. Effect of the remainder of the medium is replaced by boundaries as shown in Figure 6.1. As analysis, the following hypotheses are made:

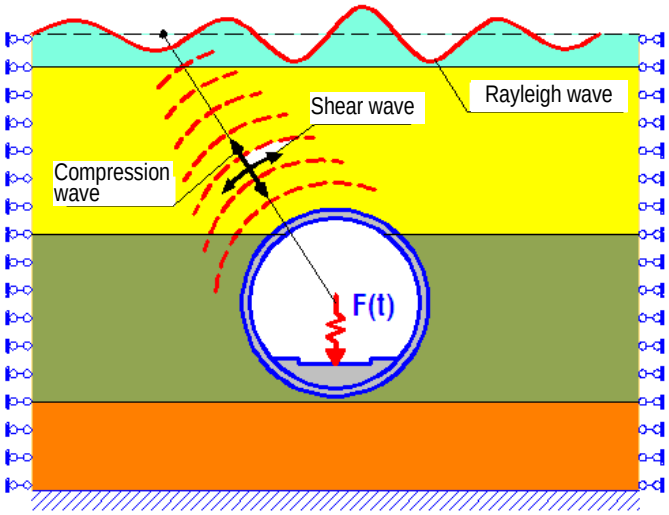


Figure 6.1 Schematic simplified the model of train-track-tunnel problem

1. Structural material is elastic.
2. Soil is modelled to be elastic plastic material. The mechanical properties of soil layers are different and in one layer is the same.
3. Displacement and strain at any position of structure-medium system is small. This hypothesis is acceptable due to much more stiffness of tunnel structure than that of soil.
4. Under the loading, displacement on interface between soil layers and between structure and soil layer as well satisfy continuous condition and thus, relatice separation and shear on them is not occurred.
5. Structure-medium system is in 2-D plane state, the system receives the vibration as load passing the study position.

6.1.3 Basic of FEM on Tunnel-Soil Interaction Problem

Under the dynamic loading, the motion differential equation of elements is (Fadeev, 1995; Bathe, 1982; Zienkiewicz et al., 2000).

$$[M]_n\{\ddot{U}\}_n + [C]_n\{\dot{U}\}_n + [K]_n\{U\}_n = \{R\}_n \quad (6.5)$$

Here:

$[M]_n, [C]_n, [K]_n$: mass matrix, damping matrix, and stiffness matrix of element

$\{\ddot{U}\}_n, \{\dot{U}\}_n, \{U\}_n$: acceleration, velocity, and displacement vector of node

$\{R\}_n$: nodal load vector

The matrices of element including $[M]_n, [C]_n, [K]_n$ are estimated in the local coordinate system. To estimate the motion equation of total system, movement equation of element in the local coordinate system should be transferred to that in the global one by transfer matrix. After transformation, the equation of element in global coordinate system is rewritten as following.

$$[\bar{M}]_n\{\ddot{\bar{U}}\}_n + [\bar{C}]_n\{\dot{\bar{U}}\}_n + [\bar{K}]_n\{\bar{U}\}_n = \{\bar{R}\}_n \tag{6.6}$$

Here:

$[\bar{M}]_n, [\bar{C}]_n, [\bar{K}]_n$: mass matrix, damping matrix, and stiffness matrix of element in global coordinate system

$\{\ddot{\bar{U}}\}_n, \{\dot{\bar{U}}\}_n, \{\bar{U}\}_n$: acceleration, velocity, and displacement vector of node in global coordinate system

$\{\bar{R}\}_n$: nodal load vector in global coordinate system

Using direct stiffness method to assemble the element into system, from (6.2) the motion equation of system is obtained as following (Fadeev, 1995; Lai, 2005; Ta, 2005; Bathe, 1982; Zienkiewicz et al., 2000).

$$[\bar{M}]\{\ddot{\bar{U}}\} + [\bar{C}]\{\dot{\bar{U}}\} + [\bar{K}]\{\bar{U}\} = \{\bar{R}\} \tag{6.7}$$

Here:

$[\bar{M}], [\bar{C}], [\bar{K}]$: mass matrix, damping matrix, and stiffness matrix of system in global coordinate system

$\{\ddot{\bar{U}}\}, \{\dot{\bar{U}}\}, \{\bar{U}\}$: acceleration, velocity, and displacement vector of node in global coordinate system

$\{\bar{R}\}$: nodal load vector in global coordinate system

The matrix $[\bar{C}]$ represents the material damping of the materials. In reality, material damping is caused by friction or by irreversible deformations (plasticity or viscosity). With more viscosity or more plasticity, more vibration energy can be dissipated. If elasticity is assumed, damping can still be taken into account using the matrix $[\bar{C}]$. To determine the damping matrix, extra parameters are required, which are difficult to determine from tests. In finite element formulations, $[\bar{C}]$ is often formulated as a function of the mass and stiffness matrices (Rayleigh damping) as:

$$[\bar{C}] = \alpha_R[\bar{M}] + \beta_R[\bar{K}] \tag{6.8}$$

Rayleigh coefficients are determined by means of natural frequency f_i, f_j and correlated damping ratio by equation system as following:

$$\begin{Bmatrix}\alpha_R \\ \beta_R\end{Bmatrix} = \begin{Bmatrix}\frac{2(h_i f_i - h_j f_j)}{f_j^2 - f_i^2} f_i f_j \\ \frac{2(h_i f_i - h_j f_j)}{f_j^2 - f_i^2} f_i f_j\end{Bmatrix} \tag{6.9}$$

In general, effect of high natural frequency on damping ratio is not remarkable. Therefore, the damping ratio is assumed to be constant and the calculation considers the first and the second natural frequency of system (Fadeev, 1995; Lai, 2005; Ta, 2005; Bathe, 1982; Zienkiewicz et al., 2000).

$$\begin{Bmatrix}\alpha_R\\ \beta_R\end{Bmatrix} = \begin{Bmatrix}\frac{2h}{f_1+f_2} f_1 f_2\\ \frac{2h}{f_1-f_2}\end{Bmatrix} \tag{6.10}$$

As combined with boundary condition, the equation (6.7) becomes:

$$[M]\{\ddot{U}\} + [C]\{\dot{U}\} + [K]\{U\} = \{R\} \tag{6.11}$$

With elestic material, Properties of the material depend on elastic modulus, E and poison ratio, υ. Thus, the matrices in (6.11) is not changed during loading. With material behavour as elastic plastic, visco-elastic, stress of the material depends on strain and deformation. Therefore, the stiffness and damping matrices of system depend on displacement vector of node. Hence, (6.11) can be rewritten as following:

$$[M]\{\ddot{U}\} + [C\{U\}]\{\dot{U}\} + [K\{U\}]\{U\} = \{R\} \tag{6.12}$$

The dynamic equilibrium equations of structure-ground system, (6.11) and (6.12) have the unknowns of node displacements. After solving the equations and using relations of finite element, the displacement, stress, and strain of each element will be obtained. At present, many methods of previous researchers have been proposed for the problem. Bathe and Wilson (1973 & 1982) reported that Newmark method is simple and practical above all others for calculation with stability and accuracy. Generally, to solve the equation (6.12), iterative procedure based on linear solution should be used. The stress and strain are redistributed and the correlative matrices are reformed at each iteration step of each increment in process. The recalculation until the equilibrium balance of stress-strain state at all position of system is restored. Such methods are therefore referred to as Newton-Raphson methods and widely used in nonlinear analysis. In today's solution, the direct integration method of Newmark combined with the Newton-Raphson iteration method is used (Lai, 2005; Ta, 2005, Bathe, 1982).

6.2 ANALYSIS PROCEDURE

In order to predict the ground-borne vibration due to moving train on metro system in Hanoi city, a 2D finite element model was developed in this study. Plaxis is a program based on finite element method (FEM). The program was originally developed at the University of Delft in Netherland where research in geotechnical design based on FEM in the '70s resulted in a commercial version of the program in 1987 and since 1998 it is available in a Windows version with a user-friendly interface. The program can simulate problems with the most common construction element such as beams and struts. Today, the program is practical for solving most complex geotechnical problems. The program is divided into four sub-programs (Input, Calculation, Output and Curves) (Brinkgreve et al., 2006). From these features, use of Plaxis in geotechnical design works has been becoming widely in Vietnam at present.

However, as using Plaxis in order to solve problems of soil-tunnel interaction under dynamic loading induced by moving train, the program has not sufficiently provided calculation tools as following:

1. Dynamic load described in the program is harmonic ones and other cases of load including train-induced dynamic load require the definition by user.
2. The module for calculation of natural frequency of system in order to estimate the damping matrix in (6.8) has not been available in the program. The user must provide the Rayleigh coefficients as equation (6.10)

Therefore, to use effectively the program for the prediction of ground-borne vibration due to train-induced dynamic loading on tunnel in Vietnam, the objectives of this study is to improve the aforementioned issues.

1. Making a model to simulate the dynamic loading of moving train to be the input data for Plaxis program
2. Proposing a method for determination of the nature frequency of analysis model to provide for Plaxis the two Rayleigh coefficients

From the above background, this study has proposed an analysis procedure for the ground-borne vibration prediction as shown in Figure 6.2. Essentially, the following problems has been performed in this study

1. Model and simulate the dynamic load of metro train
2. Model and simulate the tunnel-soil interaction problems

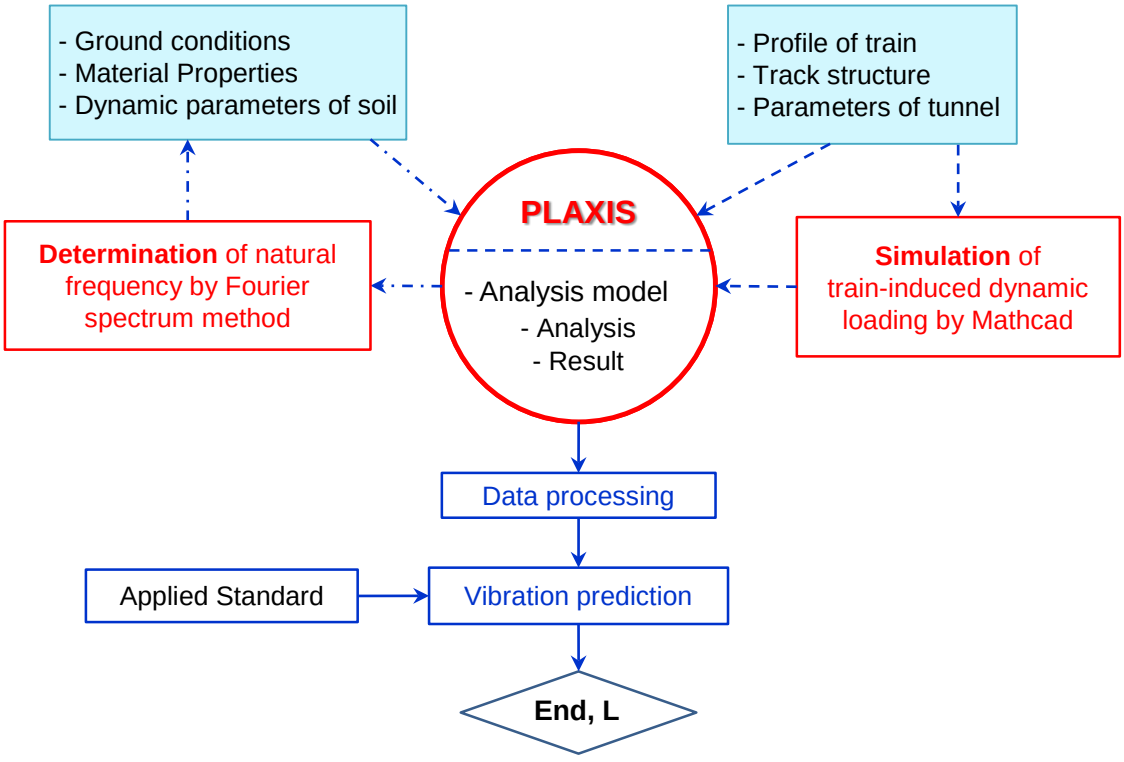


Figure 6.2 Schematic diagram of prediction procedure for train-induced vibration from tunnel

6.2.1 Selection of material model

Generally, medium model is the set of relations describing properties the medium in a process. The model should allow using mathematical language to describe the fundamental behaviors of the medium under loading with high accuracy and reliability. Nowadays, many sophisticated medium models can simulate soil behaviors, which is varied its state during loading. The models with other variables have being improved together with progress of scientific and technology. However, models should be as simple as possible and as accurate as necessary regarding the task they serve. With soil model, it should describe main properties of soil, uniquely defined in term of mathematics and be easy for use of mathematical function. In addition, the model should be practical in current condition, which requires the soil parameters for input data as few as possible.

Recently, based on the results of study on soil kinds in South Asia area by Plaxis and experiment, Ahmad (2010) and Bahatin (2008) have reported that Mohr Coulomb model and Hardening Soil model agree well with experiment results and shows almost not any distinction in analysis with friction soils. Bui (2007) proposed use of modified Cam Clay model for weak soil layers in Hanoi area. Moreover, the soil parameters for the Mohr Coulomb and modified Cam Clay models can be obtained from data of geologic survey reports in current condition of Vietnam. Therefore, this is the reason why this study use modified Cam-Clay model for weak soil and Mohr-Coulomb for other soil to analyze in Plaxis.

The models and their parameters described in detail can be availably found in literature (Fadeev, 1995; Brinkgreve et al., 2006; Kojic, 2005; Helwany, 2007). The parameters of the models for analysis in Plaxis can be classified into two groups, basic parameters and particular ones of each model. The basic parameters can be easily obtained from basic test of soil samples such as unit weigh (ρ), two Rayleigh coefficient (α_R & β_R), friction angle (φ), cohesion (c), and dilatancy angle (ψ). $\psi \approx 0$ is for overconsolidated soil, clay; $\psi \approx \varphi - 30^0$ is for sand; $\psi \approx 0$ is for soil kinds with $\varphi \approx 0$ (Brinkgreve, et al., 2006).

Mohr-Coulomb model parameters:

Beside the aforementioned parameters, Mohr-Coulomb model requires more two parameters including Young modulus (E_{eq}), Poisson's ratio (ν) as shown in Figure 6.3, which can be obtained from geologic survey reports or basic test of soil sample. The two parameters can be estimated in Plaxis by means of equation (5.1), (5.2), and (5.3) as providing shear wave velocity (v_s) and compressive wave velocity (v_p).

Modified Cam-Clay model parameters:

Modified Cam Clay model was made based on five particular parameters as shown in Figure 6.4. The parameters including Poisson's ratio (ν_{ur}), Cam-Clay swelling index (κ), Cam-Clay compression index (λ), Tangent of the critical state line (M), initial void ratio (e_{init}) can be obtained from basic test of sol sample. Poisson's ratio ν_{ur} is a real elastic parameter and not a pseudo-elasticity constant as used in the Mohr-Coulomb model. Its value will usually be in range between 0.1 and 0.2 (Brinkgreve, et al., 2006). Compression index and swelling index can be obtained from one-dimensional consolidated compression test as following:

$$\lambda = \frac{C_c}{ln10} \text{ and } \kappa = \frac{C_s}{ln10}) \quad (6.13)$$

The parameter M should be based on the friction angle and estimated from plastic condition of Mohr-Coulomb as following:

$$M = \frac{6.sin\varphi}{3-sin\varphi} \quad (6.14)$$

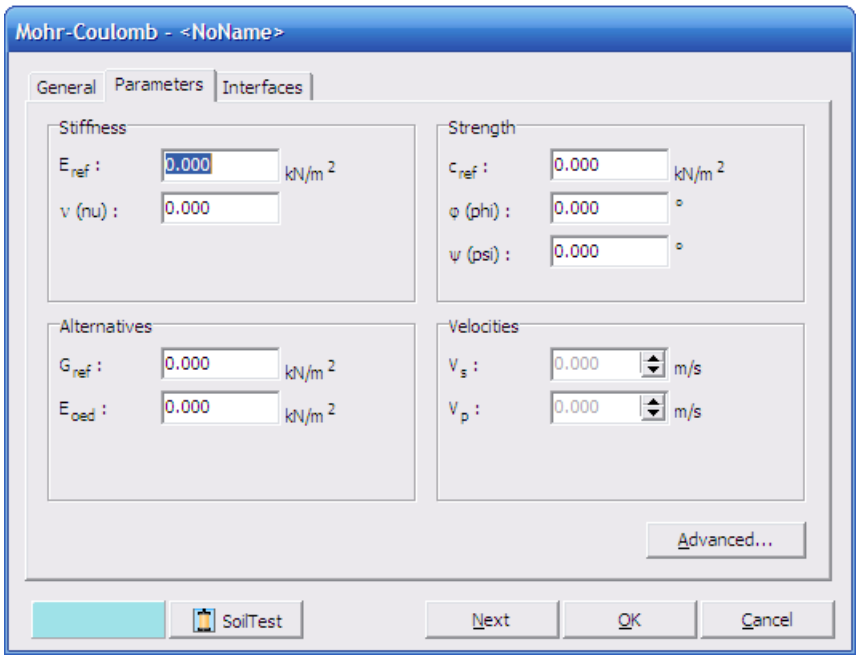


Figure 6.3 Mohr-Coulomb model parameters in Plaxis

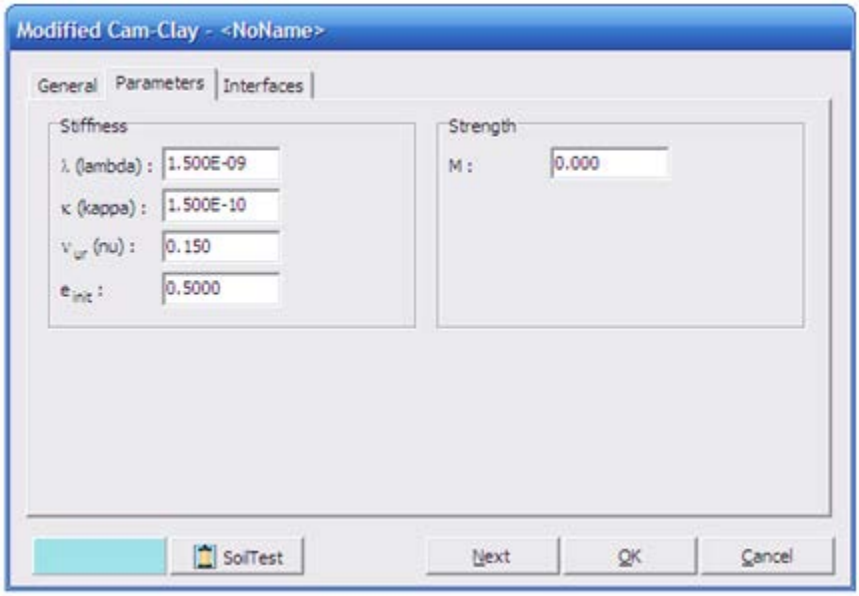


Figure 6.4 Cam-Clay model parameters in Plaxis

6.2.2 Simulation of moving train load

Dynamic loadings emitting vibration (source) induced by passing train is governed by numerous factors which are strongly depended on parameters such as how smooth the wheels and rails are and the resonance frequencies of the vehicle suspension system and the track support system. The factors are extremely complex, which may be quantitatively determined not only by merely theoretical model but also by measurement results for validation of the model. In today' solution, there are three approaches to describe the dynamic loading of metro train, depended on objective of vibration calculation, computing tool and availability of experimental equipment. In the first approach – theoretical method, Hussein et al. (2006, 2009), Jia et al. (2008) have used mathematical tools to model the moving train load by a function as F(x,y,z,t). The method is applicable to simulate in the case of most tunnel and track system as well with acceptable errors. Hung et al. (2000) have solved the problem by decoupling the train from the track-soil system. Di et al. (2007), Rajib et al. (2008) have developed a train-rail interaction model in consideration to suspensions of car, rail pad and so on. Generally the equation of loading function in the studies is described as a simplified or elaborated periodic oscillation function. The authors used the different load functions in conformity with their analytic or numerical calculation tools and 2D or 3D models. In the second approach – experimental method, Fujii et at. (2005), Pakbaz et al. (2009) have performed study on vibration prediction from existing metro line by a numerical analysis model combined with data from acceleration measurement equipment attached on tunnel floor, rail, underground and ground surface during passing train with different speeds. Because of use of the measurement data, the results of the model can accurately estimate the dynamic loading. However, it is applicable for only one type of train and track system in particular case. In other cases, as the parameters are varied, the results are not appropriate to be applied. Based on third approach – theoretical method combined with experiment, the previous researchers have used the mathematical equation to describe loading function of train F'(x,y,z,t) = Ψ.F(x,y,z,t). Where Ψ is estimated from experiment results by comparing Ψ.F(x,y,z,t) with measurement data. Chai et al. (2008) have described the loading function as following:

$$F(y,t) = Q(t).\delta(y - vt) \tag{6.15}$$

Where:

$$Q(t) = Q_0(1 + \gamma_1 cos\Omega_1 t + \gamma_2 cos\Omega_2 t) \tag{6.16}$$

v: velocity train

Q_0: average contact pressure between wheel and rail

Ω_1, Ω_2: Angular frequency of slab and fastener, respectively

γ_1, γ_2: Two ratio estimated by experimental data

Stemming from above discussion based on literature review in consideration to condition of Vietnam, the modelling method using mathematical tools in order to describe the train-induced dynamic loading should be auspicious at current time. In a typical model, the entire system of railway components is divided into two subsystems, the train and the track, between which there is a possibly physical wheel-rail contact. It is common that the behaviors of these dynamic subsystems are investigated quite separately. Such investigations may include either a complex train model together with

a simple track model or a simple train model with a complex track model (David, 2005). In the present study, the train is assumed to be modeled as a single wheel with static wheel load moving along a track in a constant speed with consideration to dynamic behavior due to the train-track interaction through irregularity between the track and the wheels by which is described a shape function of the irregularity (David, 2005). Thus, ignoring the bounce between wheel and rail and train body self-sway, relation of rail and wheel is linear with simultaneous vibration and displacement under loading. The static load representing the train mass is applied directly on the wheel without consideration of primary suspension element. The track is described by a well-known model of a continuously rail beam on elastic foundation, that has the enormous advantage of simplicity and availability of analytical solutions under loads moving at constant velocity (Hussein et al., 2006; Paolucci et al., 2003; Kenney, 1954). Thus, in order to estimate the dynamic loading on tunnel, two problems should be solved, dynamic force on rail and its distribution onto tunnel through the rail and in turn track structure such as rail pad and sleeper. It means that the loading can be split up into two parts (Hung, 2001). The first part is generated by interaction between the wheels and rails which is moving with wheels. The interaction force may be simulated by a quasi-static term of constant value plus a dynamic term that varies with time (Esveld, 1989). The static term is contributed mainly by the wheel weight, whereas the dynamic term by the track irregularities and vehicle defects, such as wheel flats, natural vibration and hunting. The second part relates to the distribution of the axle loads passing a fixed point given as a distribution loading function. In this case, the wheel load is regarded as the force exerted from the track onto the track structure and in turn tunnel floor, rather than the one from the wheels onto the track, one may use the deflection curve of the track to simulate the distribution of the wheel load (Krylov et al., 1994 & 1995; Takemiya, 1997). The track is treated as an infinite Bernoulli-Euler beam supported by the track structure without ballast as an elastic foundation with stiffness, *s* as shown in Figure 6.5. For an elastically supported beam with an axle load P=1 acting at z=0 (z is axle of rail), the distribution loading function is written as following (Bahatin, 2008; Hussein et al., 2006; Esveld, 1989).

$$\Phi(z) = \frac{1}{2\alpha} e^{\frac{-|z|}{\alpha}} \left[\cos\left(\frac{|z|}{\alpha}\right) + \sin\left(\frac{|z|}{\alpha}\right) \right] \tag{6.17}$$

Where: α: characteristic length, $\alpha = \sqrt[4]{\frac{4EI}{s}}$ (6.18)

EI: bending stiffness of track

s: stiffness of elastic foundation

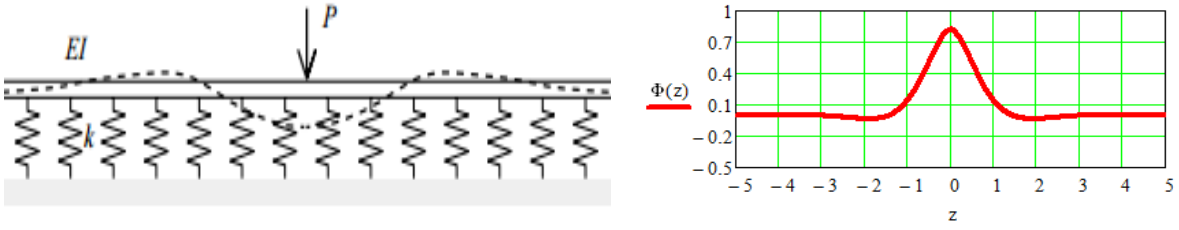


Figure 6.5 Schematic of single wheel load on track and diagram of its function according to Bernoulli-Euler

Extend the single wheel load case to the case of a train consisting of N carriages and n axles for each carriage, the total distribution function of a sequence of moving wheel loads can be written as:

$$\Phi(z) = \sum_{i=1}^{N}\sum_{j=1}^{n}\Phi_{ji}(z) \tag{6.19}$$

Be combined with the first part, the general loading function of a moving train can be expressed as:

$$F(z) = \sum_{i=1}^{N}\sum_{j=1}^{n}P_{ji}(z).\Phi_{ji}(z) \tag{6.20}$$

Where:

$P_{ji}(z)$: interaction force between wheels and rail of i^{th} axle in j^{th} at z coordinate, including the static term of the axle weight and the dynamic term due to the irregularities and wheel defects

$\Phi_{ji}(z)$: distribution loading function of i^{th} axle in j^{th} at z coordinate

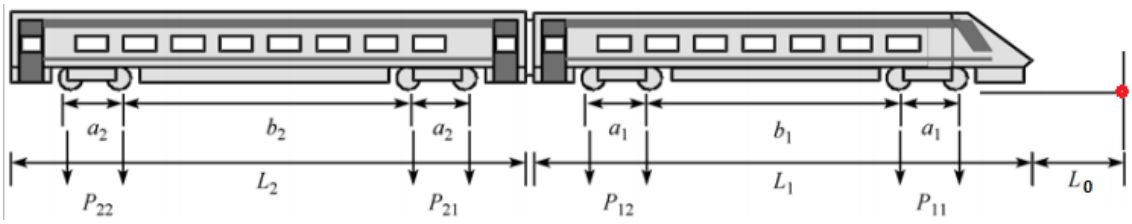


Figure 6.6 Geometric profile of train wheel loads

To describe the moving train load, convert from the z coordinate into time coordinate by replacing z with $v(t-t_0)$ where v is the train velocity and t_0 is the time that the first axle running to reference position as shown in Figure 6.6, combine (6.17) and (6.20), the moving train load is expressed as:

$$F(t) = \sum_{i=1}^{N}\left[\begin{array}{l}\left[P_{1i}^{Sta} + P_{1i}^{IR}\left\{v(t-t_0) - \sum_{j=0}^{i-1}L_j\right\}\right].\Phi\left\{v(t-t_0) - \sum_{j=0}^{i-1}L_j\right\} \\ + \left[P_{2i}^{Sta} + P_{2i}^{IR}\left\{v(t-t_0) - \sum_{j=0}^{i-1}L_j - a_i\right\}\right].\Phi\left\{v(t-t_0) - \sum_{j=0}^{i-1}L_j - a_i\right\} \\ + \left[P_{3i}^{Sta} + P_{3i}^{IR}\left\{v(t-t_0) - \sum_{j=0}^{i-1}L_j - a_i - b_i\right\}\right].\Phi\left\{v(t-t_0) - \sum_{j=0}^{i-1}L_j - a_i - b_i\right\} \\ + \left[P_{4i}^{Sta} + P_{4i}^{IR}\left\{v(t-t_0) - \sum_{j=0}^{i-1}L_j - 2a_i - b_i\right\}.\right]\Phi\left\{v(t-t_0) - \sum_{j=0}^{i-1}L_j - 2a_i - b_i\right\}\end{array}\right] \tag{6.21}$$

Where:

L_j, a_i, b_i: Car length, distance between axles of i^{th} car, respectively as described in Figure 6.6

P_{ki}^{sta}: Static load of k^{th} axle *(k=1÷4)* in i^{th} car [kN]

$P_{ki}^{IR} = M_{0_{ki}}\zeta(z)\omega_{ir}^2$: Inertia force of axle caused by rotating mass below primary suspension (Jia et al., 2008; Qui et al., 2007) [kN]

$M_{0_{ki}}$: Weight of the rotating mass of k^{th} axle in i^{th} car, excluding mass above primary suspension

$\omega_{ir} = 2\pi f_{ir}$: Radian frequency of primary suspension component

$f_{ir} = \frac{v}{L_{ir}}$: Random frequency due to irregularities between wheel and rail

In case of the new metro line being under construction that is not operated and lack of measure data, to predict the vibration the frequency may be computed in term of mean frequencies in random frequency band, the one-third-octave bands of 8Hz, 16Hz, 31.5Hz, 63Hz (FTA, 2006; SP, 2004). This is accordance with Russia standard being used in Vietnam, which the vibration frequencies of train-induced loading on tunnel usually appear within range of 0÷80Hz.

$\zeta(z) = \frac{a_{ir}}{2}\left[1 - cos2\pi\frac{z}{L_{ir}}\right]$: Deviation equation of contact interface between wheel and rail (David, 2005)

$a_{ir} = 0.2 \div 0.4$ mm: Defect depth of rail (David, 2005; Dahlberg, 2003)

L_{ir}: Wavelength on railhead due to irregularities, Alias (1986) gives an overview of different types of wave formations on the railheads. The irregularities are divided into three categories: corrugation, with wavelength 30 to 80 mm and with amplitudes of a few hundredths of mm; short wave, with wavelength 150 to 300 mm and with amplitudes up to 1 mm; and long wave, with wavelength up to two meters.

In the present study, the track structure is designed without ballast. The concrete slippers, is rested directly on tunnel floor, support the rail through rail-pad. Because of large stiffness of the tunnel floor, *s* is assumed as stiffness of the rail pad supporting uniformly one unit of rail length. Thus, s can be computed as following.

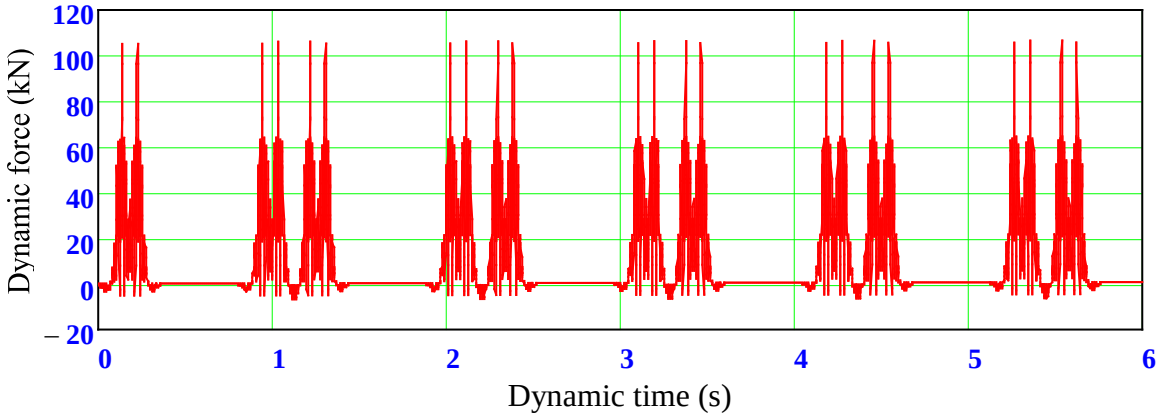
$$s = \frac{k_{rail-pad}}{L_f} \tag{6.22}$$

Where:

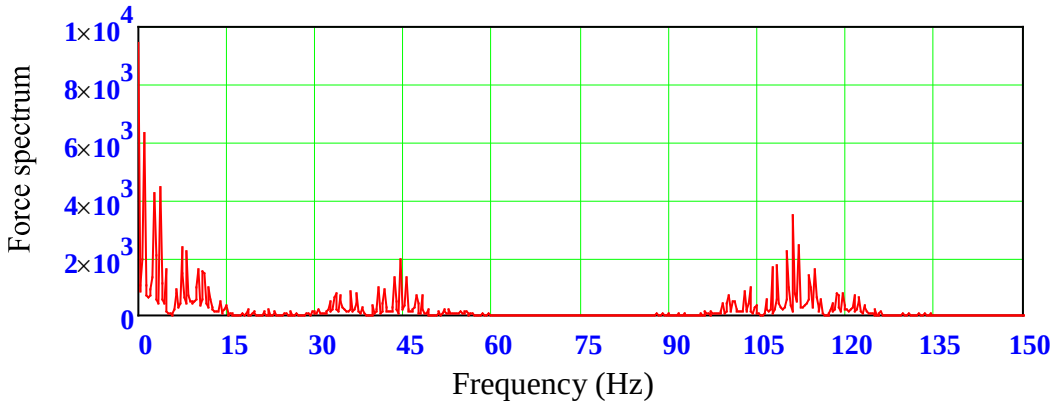
$k_{rail-pad}$: stiffness of rail-pad

L_f: space between slippers

The numerical simulation procedure stated above is accomplished in software Mathcad by programming and presented in Appendix A. The calculation parameters of the train and track structure of the metro line No.3 project in Hanoi were used for this analysis. The train named Metropolis 98 is composed of 6 cars with length L = 24 m and total mass 490.92 kN for each car, where each car has two bogies separated by distance b = 16 m, each of which in turn comprises two axles, i.e. two sets of wheels, separated by distance a = 2 m. The mass of one axle is M_0 = 15.03 kN. The track system namely UIC60 was used in this study with rail modulus of 2.07×10^5 MPa, the sleeper space of 0.65 m, and rail pad elastic stiffness of 1.2×10^5 kN/m. The wavelengths of $L_{ir.1}$= 0.2 m; $L_{ir.2}$= $0.2\pi.D_w$ (D_w is wheel diameter) and the defect depths of $a_{ir.1}$ = 0.25 mm; $a_{ir.2}$ = 1 mm were assumed in this analysis. The numerical result of the dynamic load applied to the tunnel is obtained as shown in Figure 6.7.



a. Dynamic load on tunnel from one rail



b. The spectrum of the dynamic force from one rail

Figure 6.7 Characteristic of the dynamic load applied to the tunnel

The above Figures describe the calculated dynamic load and frequency spectrum when the train speed is 80 km/h, which clearly show that the force is mainly induced by the moving axle loads of train, and that the load mainly concentrates at the frequency range of 0 to 15 Hz, 30 to 50 Hz and 100 to 125 Hz. This is consistent with previous researches reported by Gupta et al., 2007. Accordingly, this load in term of time history is adopted as the dynamic load for next calculation.

6.2.3 Determination of natural frequencies of multi-layered ground

As above discussed, the module for calculation of natural frequency of system has not been availably integrated in the Plaxis. In order to estimate the damping matrix as in (6.8), the engineers are required to provide the two Rayleigh coefficients as Equation (6.10). Therefore, this study has utilized the Fourier amplitude spectrum method to analyze the seismic problem in consideration to the damping of soil. The fundamental principal of the method is excitation of a constrained vibration into the system, then determination of free vibration and transformation into Fourier spectrum in order to estimate the nearly resonant vibration frequencies which are assumed as the natural frequencies of the system.

To excite the vibrated system, in numerical analysis, the earthquake loading is usually chosen as a time-history ground acceleration which is introduced at the lower boundary of the model (Kramer, 1996). This study used the earthquake data availably integrated in Plaxis as an excitation source of vibration as shown in Figure 6.8.

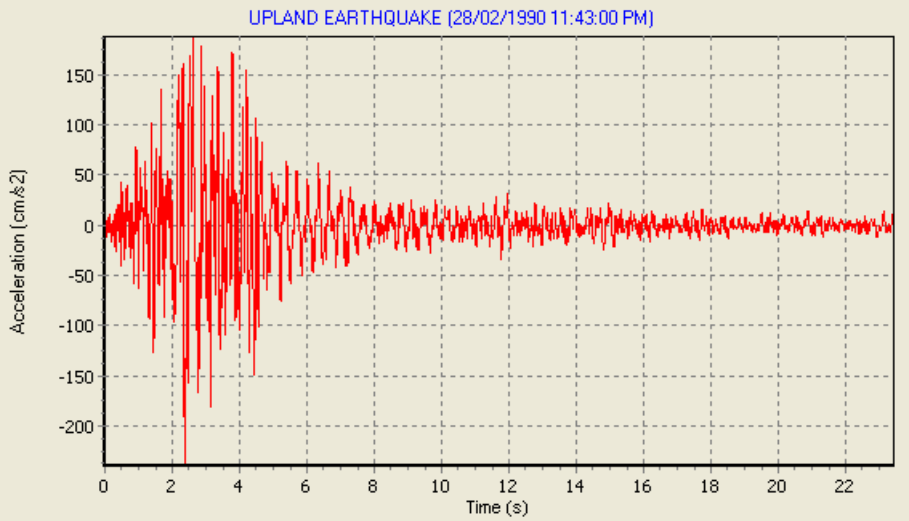


Figure 6.8 Input excitation

Fourier transform for a discrete valued series is called Fast Fourier Transform algorithm (FFT).

With a discrete valued series with *N* samples corresponded with displacement datum into time interval Δt as:

$$u(t_k) = [u_0, u_1, \dots, u_k, \dots, u_{N-1}]; \quad k = 0,1, \dots, N-1 \;\&\; t_k = k.\Delta t \tag{6.23}$$

Fast Fourier Transform of (6.23) with n^{th} (ω_n) frequency is expressed as:

$$U(\omega_n) = \Delta t \sum_{k=0}^{N-1} u(t_k) e^{-i\omega_n t_k}; \quad \omega = n.\Delta\omega = \left(\frac{2\pi n}{N}\right)\Delta t \tag{6.24}$$

Application of the Euler's relation, (6.24) is rewritten as:

$$U(\omega_n) = \Delta t \sum_{k=0}^{N-1} [u(t_k).cos(\omega_n t_k) - i.u(t_k).sin(\omega_n t_k)] \tag{6.25}$$

Equation (6.25) may be analyzed in term of function with specific frequency:

$$U = U_{real} + iU_{imag} \tag{6.26}$$

Where: U_{real}, U_{imag}: real part and imaginary part corresponding to each radian frequency, ω_n or frequency, f_n

Thus, Fourier amplitude spectrum is defined as:

$$FS(f) = \sqrt{(U_{real})^2 + \left(U_{imag}\right)^2} \tag{6.27}$$

The FFT calculation procedure is implemented by Exel with the steps as shown in Figure 6.9.

Firstly, a finite element model was made in Plaxis. To obtain a realistic response of the give system subjected to seismic loading, it is necessary to choose the optimum parameter such as geometry, domain width, meshing, and parameters of numeric

time-integration for the model without jeopardizing the reliability and rational feasibility of the prediction. Recently, there have been some researches on effect of the parameters to the result of problem of single layer of homogeneous linear elastic soil bed without damping (Arindam, 2011; Ciro et al., 2008). The researchers have been used the method that is based on the analytic solution of Kramer (1996) to validate their calculated results. Thus, based on the conclusion of the studies, the present study suggests using the parameters for the model as following:

1. B/H (B, H is the width and height of the model) ratio should be more than 15
2. The average dimension of element is $L_e = \sqrt{\frac{B.H}{n}} \leq 0.55\frac{v_s}{f}$, where n is amount of element in the model, v_s is shear wave velocity, f is maximum frequency of interest.
3. Newmark numeric time-integration parameters are $\alpha = 0.25(1+\gamma)^2, \beta = 0.5 + \gamma$, γ belong to interval $\left[0, \frac{1}{3}\right]$, assuming $\gamma = 0$ (Bathe, 1973 & 1982; Brinkgreve, 2006)

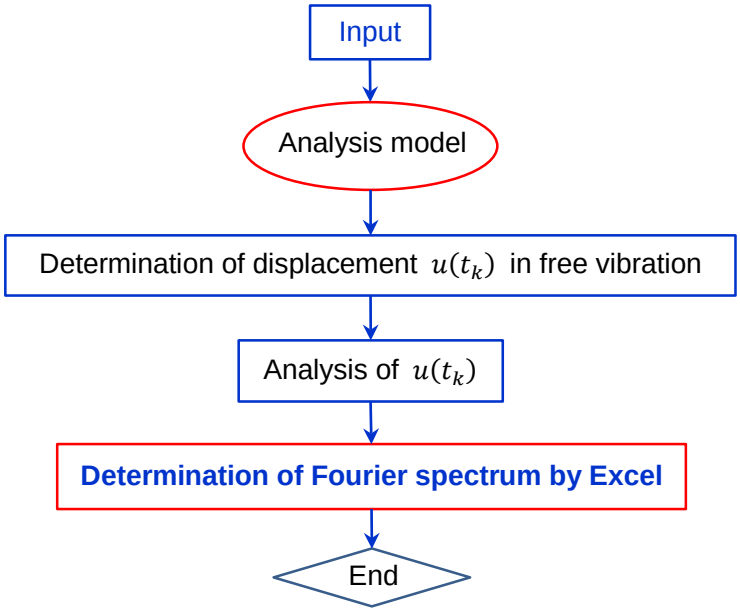


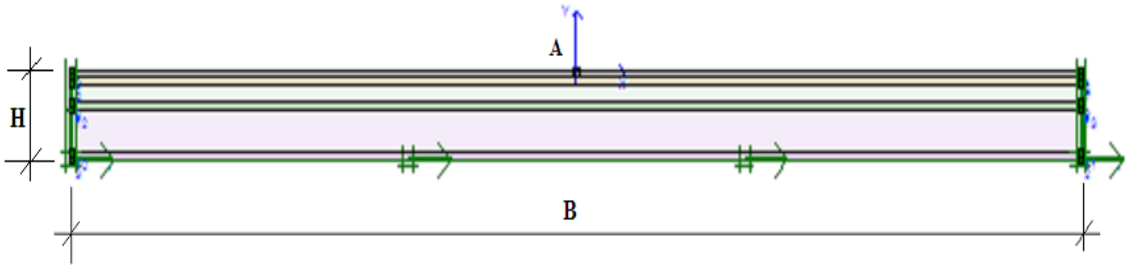
Figure 6.9 Procedure for determination of natural frequency in Plaxis

Besides the above consideration, to apply the Fourier spectrum method for the multilayered ground problem, the influences of distribution of soil layers and damping on the results need to be considered.

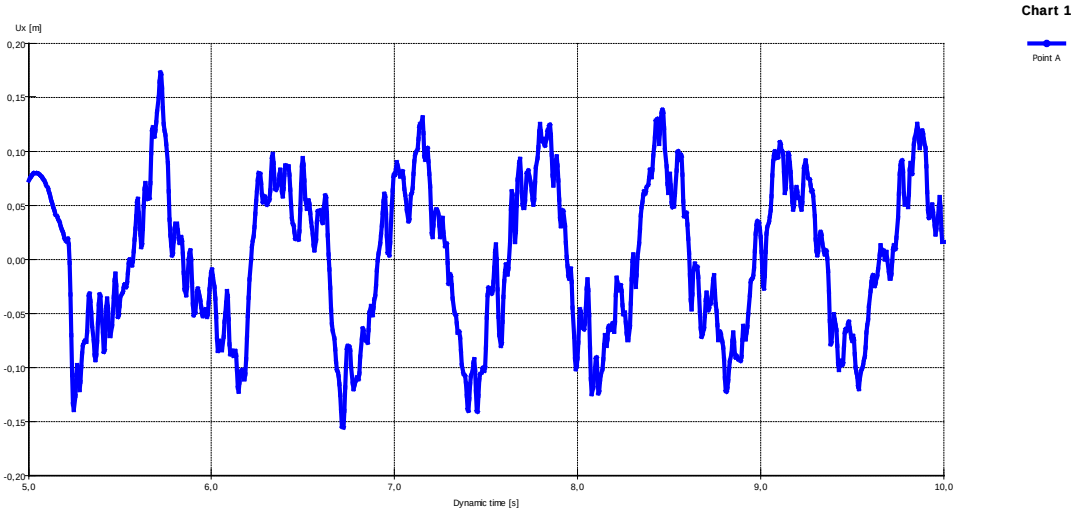
6.2.3.1 Determination of natural frequencies for Metro line No.3

Figures 6.10a and 6.11a show the analysis models for two positions Km0+940 and Km6+700, respectively of the metro line number No.3 of Hanoi city. The dynamic parameters of soil layers were used from the calculated results in the Table 5.7 and 5.8. The models were used the standard boundary condition of Plaxis, which is vertically free displacement and horizontal fixity at far-end vertical boundaries and total fixity i.e. both horizontal and vertical fixities for the bottom boundary. Absorbent boundaries were

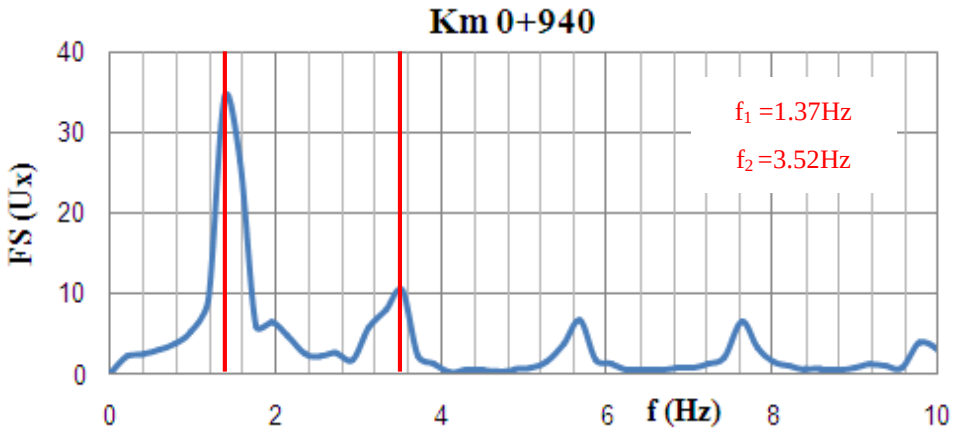
introduced at the far-vertical ones aiming to absorb the increments of stresses on the boundaries caused by dynamic loading, that otherwise would be reflected inside the soil body. The analysis results of U_x at A(0,0) on the ground surface in the case of not consideration to damping of soil are shown in Figure 6.10 and 6.11.



a. Finite element model utilized in Plaxis (H = 50 m, B/H=15)

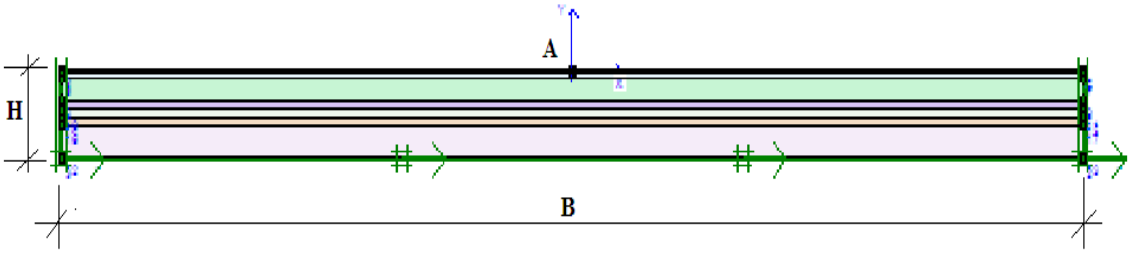


b. Diagram of free vibration without damping of U_x at A(0,0)

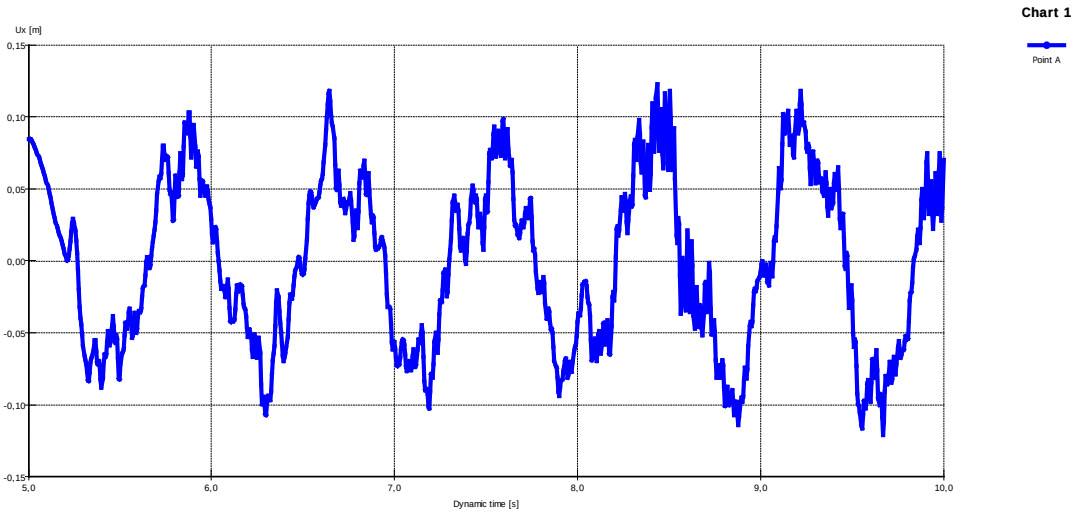


c. Analysis result FFT of U_x at A(0,0)

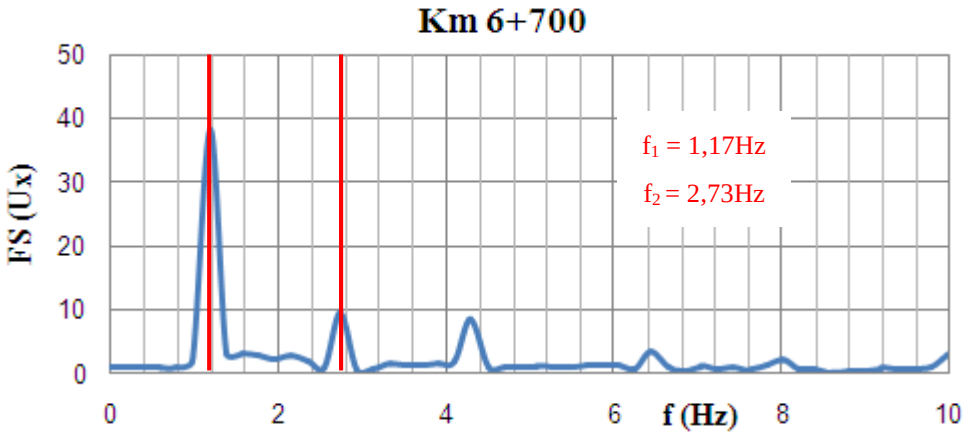
Figure 6.10 Determination of natural frequency of ground at Km0+940



a. Finite element model utilized in Plaxis (H = 50 m, B/H = 15)



b. Diagram of free vibration without damping of U_x at A(0,0)



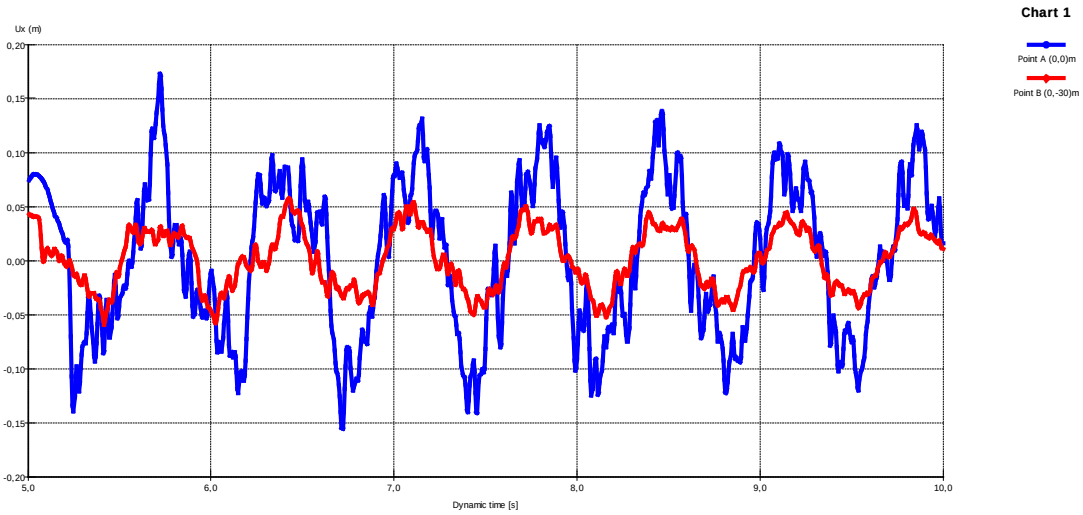
c. Analysis result FFT of U_x at A(0,0)

Figure 6.11 Determination of natural frequency of ground at Km6+700

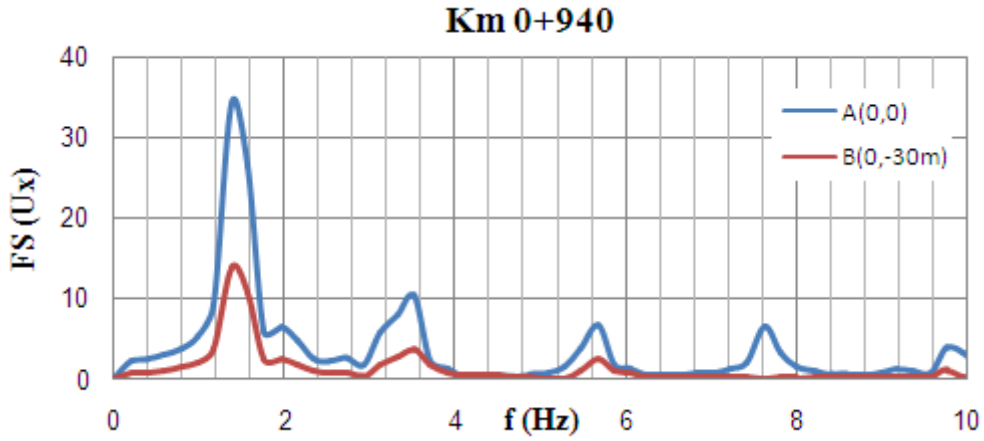
6.2.3.2. Influence of multi-layered ground and damping of soil

Figure 6.12 show the analysis results of U_x at A(0, 0) and B(0,-30m) at Km0+940 in the case of not consideration to damping of soil. It can be seen from the Figure that the natural frequencies of vibration of the system at the two points are equal, 1.37 Hz and 3.52 Hz, respectively. Thus, all points in the model are the same frequency and different amplitude. This agrees well with the results of single layer models shown in (Ciro et al.,

2008 & 2010). Since the points on the ground surface have largest amplitude of vibration, the analysis was performed for these points.



a. Diagram of free vibration without damping of U_x at A(0,0) and B(0,-30) of Km0+940

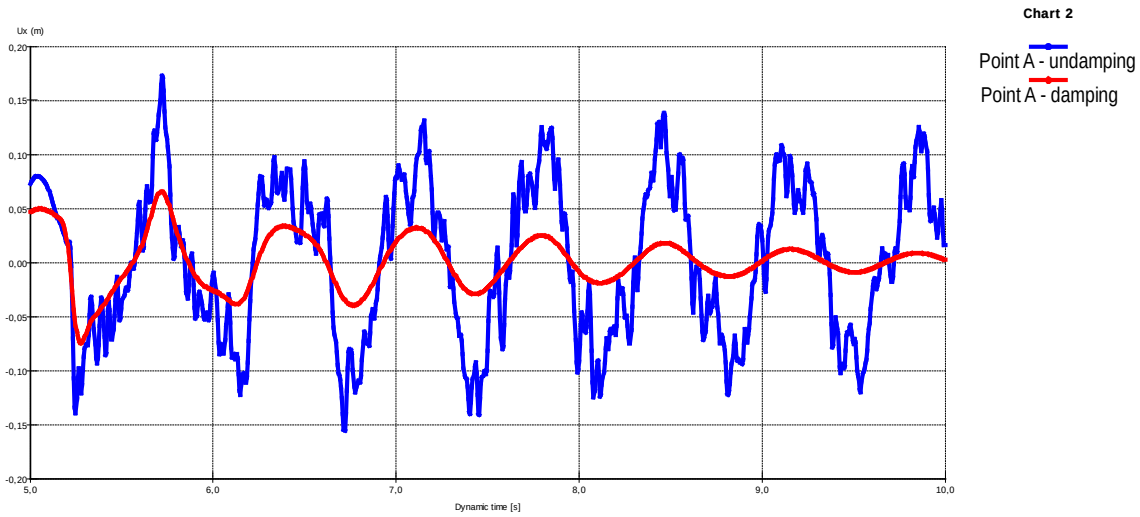


b. Analysis result FFT of U_x at A(0,0) and B(0,-30) of Km0+940

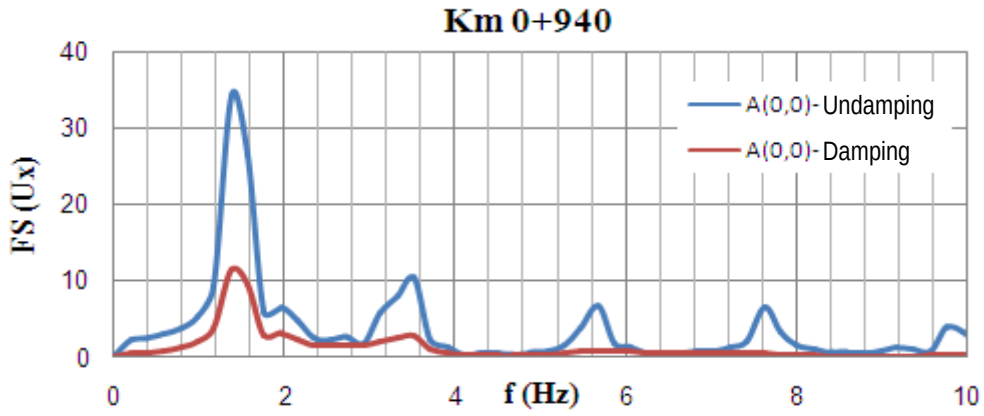
Figure 6.12 Influence of multi-layered ground on natural frequency

To evaluate the influence of damping of soil on the natural frequency by Fourier amplitude spectrum method for the multi-layered ground, the analysis procedure was performed as following:

After model analysis to obtain the first and second natural frequencies of the system without damping (damping ratio of soil layers, h = 0) as shown in Figure 6.11 or 6.12, the analysis was repeated using the two Rayleigh coefficients which were estimated for each soil layer by using Equation 6.10 with corresponded damping ration calculated in Table 5.7 and 5.8. The result is shown in Figure 6.13.



a. Diagram of free vibration with and without damping of U_x at A(0,0) of Km0+940



b. Analysis result FFT of U_x at A(0,0) with and without damping at Km0+940

Figure 6.13 Influence of damping of soil on natural frequency

The result indicates that the first and second natural frequencies of two cases with and without consideration to damping ratio of soil layers are equal. The vibration amplitude in the case of consideration to damping is smaller. Thus, to simplify, the natural frequency determination of system can be performed for model without consideration to damping of soil.

6.3 PREDICTION OF TRAIN-INDUCED VIBRATION FROM METRO LINE No.3

The metro line system of Hanoi city as operated will generate ground vibrations which cause undesirable environment and economical impacts such as nuisance of the passenger along the rail and deterioration of the alongside existing building structures. On the other hand, the train-induced vibration problem has been not sufficiently mentioned in environmental impact assessment. Therefore, the metro line No.3 was selected to analyze the train-induced vibration in this study.

6.3.1 Tunnel and ground conditions

Hanoi metro line No.3 is a part of the Hanoi metro rail system project, with starting point at Nhon town, Tu Liem district and ending point at Hanoi railway station. Generally, the geology condition of the line is good and stable in the starting area and weak in the ending area. Especially, the area from station No.6 to the ending point, around 5m depth from ground, appear a very weak soil layer with thickness from 10m to 12m (layer 1: void ratio of 2.07; water contend of 77%; plastic index of 34% and degree of saturation of 97.5%). Therefore, two typical positions of shield tunnel in the line were selected to analyze in this study. One is at Km0+940 between station No.1 and No.2 in which the tunnel is buried shallowest. Another is Km6+700 between station No.7 and end with the thickest weak soil layer. The tunnel shape and the ground profile of the two positions are shown in Figure 6.14 and 6.15, respectively. The geotechnical properties of soil layers in the line are shown in Table 6.1. The soil dynamic parameters have been calculated as shown in Table 5.7 and 5.8 of Chapter 5. The parameters of tunnel are shown in Table 6.2.

Table 6.1 Geotechnical properties of soil layers in Metro line No.3

Parameters	Symbol	Unit	Soil layer									
			F	1	1a	1b	2	2a	2b	3	3a	4
Material model	Model		MC	MCC	MC	MC	MC	MC	MC	MC	MC	MC
Unit weight	ρ	kN/m3	19,42	14,76	18,84	19,03	19,07	18,91	19,07	19,99	19,57	20,08
Horizontal permeability	k_x	m/day	2,7E+00	3,1E-03	3,2E-04	3,5E-01	3,6E-05	8,2E-04	3,6E-05	3,3E-01	3,3E-01	2,3E-05
Vertical permeability	k_y	m/day	2,7E+00	3,1E-03	3,2E-04	3,5E-01	3,6E-05	8,2E-04	3,6E-05	3,3E-01	3,3E-01	2,3E-05
Initial void ratio	e_{init}		0,6557	2,0708	0,7708	0,7167	0,7230	0,6855	0,7230	0,5664	0,6317	0,5610
Poisson's ratio	ν		0,4	0,4	0,4	0,4	0,4	0,4	0,4	0,4	0,4	0,4
Cohesion	c	kN/m2	8,92	15,72	15,72	9,88	39,72	24,27	39,72	4,48	9,86	43,52
Friction angle	φ	degree	19o00'	20o36'	20o36'	20o44'	15o29'	16o24'	15o29'	31o14'	19o42'	15o59'
Dilatancy angle	ψ	degree	0	0	0	0	0	0	0	1o14'	0	0
Interface strength reduction	R_{inter}		1	1	1	1	1	1	1	1	1	1
Plastic index	PI	%	4,60	34,00	35,10	10,90	34,00	20,00	34,00	0,00	0,00	33,10
Compressive index	Cc			0,8403								
Dilatancy index	Cs			0,2582								
Slope of failure envelope	M			0,7972								

MCC: Modified Cam-Clay Model
MC: Mohr-Coulomb Model

6.3.2 Finite element model

The finite element model is plotted in Figure 6.16. It is constituted by a rectangular domain 214 m wide and 50 m high, in order to place far enough the lateral boundaries. This should help minimizing the influence of the boundaries on the obtained results, even though no clear indications exist in literature on this aspect. Recently, Amorosi et al. (2007) have shown a case of site response analysis in which they have extended the width of the mesh eight time its height, in order to obtain acceptable results. Figure 6.16 plots the graphical boundaries condition utilized in Plaxis. Horizontal fixity has been introduced at the far-end vertical boundaries, while the bottom boundary of the model has been subjected to total fixity i.e. both horizontal and vertical fixities. Absorbent boundaries are introduced at both far-vertical and bottom boundaries. The equations of absorbent boundary are described in detail in (Nguyen, 2005; Brinkgreve et al., 2006).

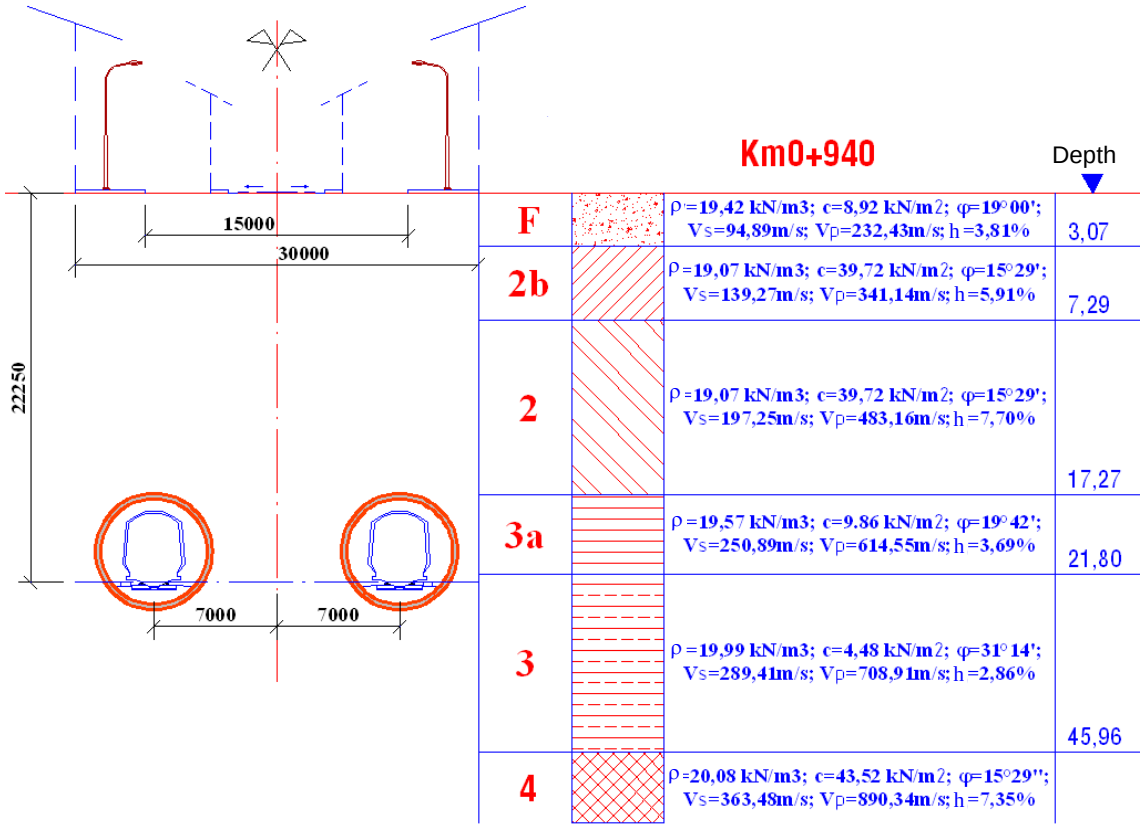


Figure 6.14 Tunnel shape and ground profile at Km0+940

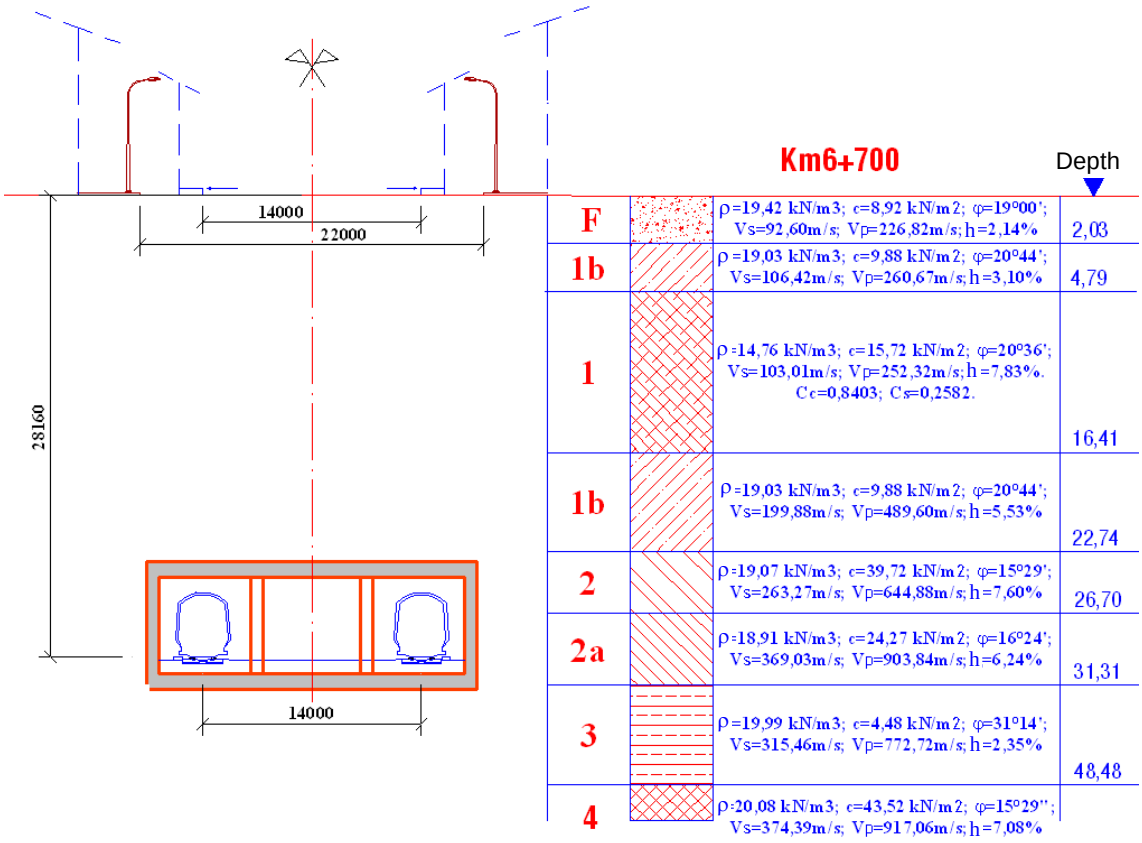


Figure 6.15 Tunnel shape and ground profile at Km6+700

Table 6.2 Parameters of tunnel

Parameters	Km0+940	Km6+700	Unit
Rail top depth	22,25	28,16	m
Tunnel type	Circle	Rectangular	
Dimension	6,0/6,6	1/0,8/1	m
Modulus of tunnel	35	35	GPa
Modulus of tunnel floor	30	30	GPa
Poisson's ratio	0,2	0,2	

Ten analyzed points on the ground surface A, B, C, D, E, F, G, H, I, J with distance of 0, 7, 17, 27, 37, 47, 57, 67, 87, 107m respectively from origin of coordinate (tunnel center line on the ground surface) are shown in Figure 6.16. The analysis procedure in Plaxis was divided into two phases. The first one is a static elasto-plastic calculation of tunnel-soil interaction without the dynamic loading (before loading). In the second phase, based on the results of stress-strain relation, displacement of the system calculated in the first phase, dynamic analysis of tunnel-soil interaction in which the loading of moving train has been simulated is performed.

In the model 15 nodes triangular elements were used infinite element mesh. For determining the optimum size of element in order to get reasonable precise result in a minimized time, four different meshing pattern were analyzed and the result of analysis with very fine and fine meshing were very close to each other therefore, fine meshing pattern were chosen as Figure 6.17.

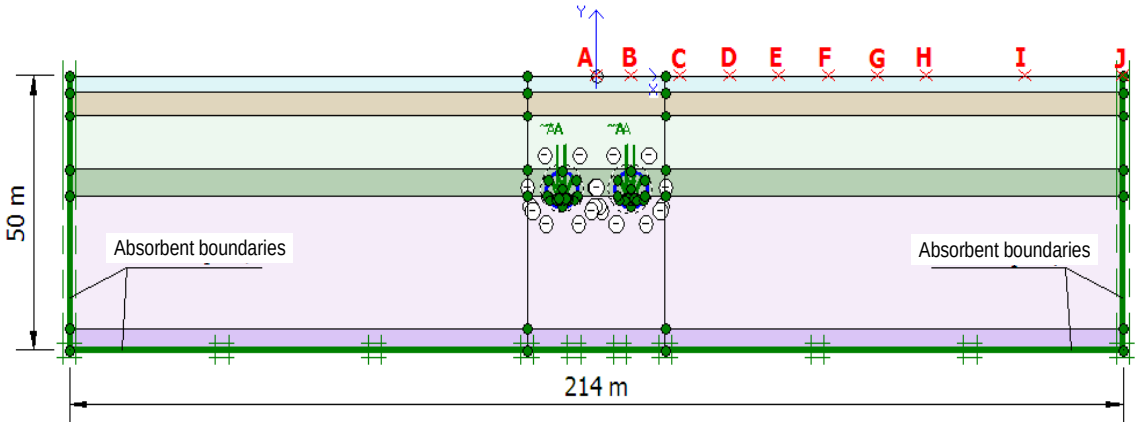


Figure 6.16 Finite element model with symmetrical loading at Km0+940

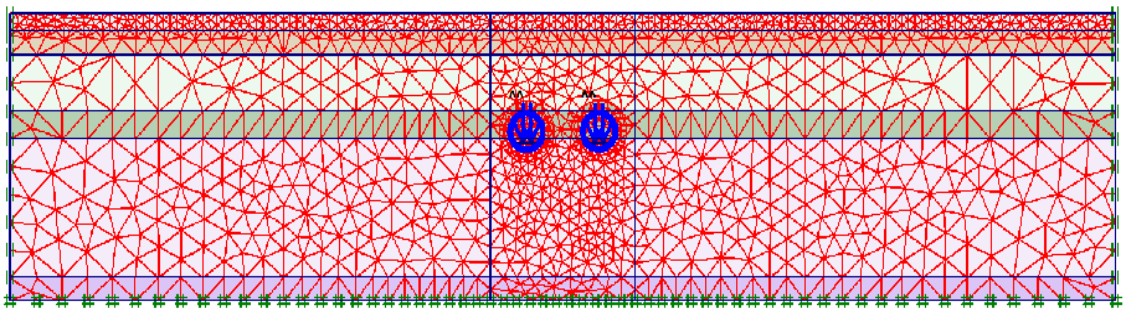


Figure 6.17 Finite element mesh

Figure 6.18 shows the results of total vibration velocity at B of Km0+940 in the case of moving double train (symmetrical loading) and single train (nonsymmetrical loading) at the position of the double hollow tunnel. It can be seen apparently that the vibration velocity caused by the double train is higher than that by the single one. Therefore, to estimate the maximum vibration level in the most unfavorable case as Equation 6.1, the numerical results obtained from the model in this study would be shown in the case of the symmetrical loading.

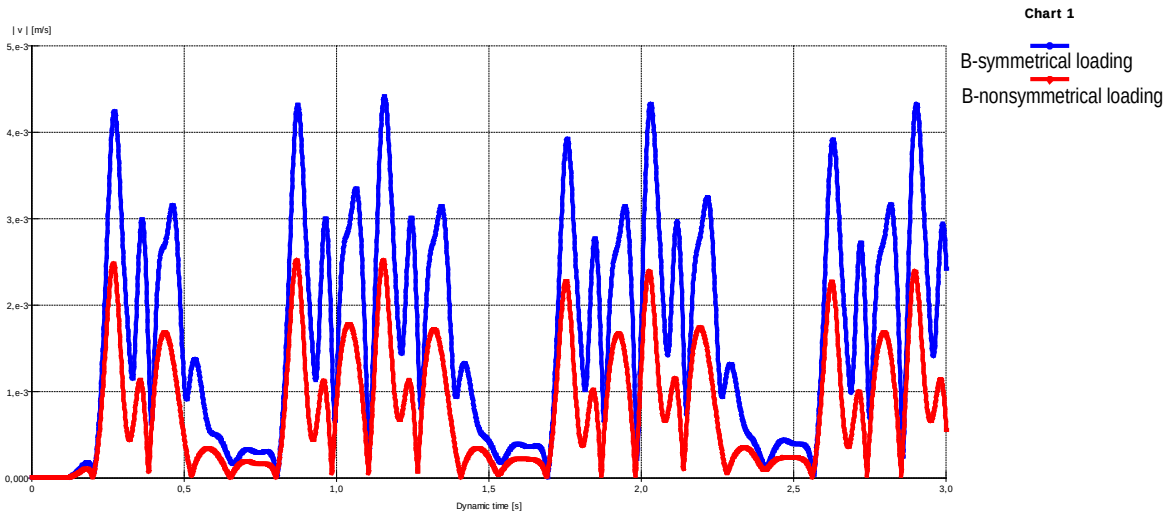


Figure 6.18 Graph of total vibration velocity with time at B with v = 80 km/h, f_{ir} = 63 Hz in the case of symmetrical and nonsymmetrical loading

6.3.3 Analysis results and discussion

6.3.3.1 Vibration level

Figure 6.19 and 6.20 respectively show vertical and horizontal vibration velocities at B and total vibration velocities at B, E, H of Km0+940 with train velocity of 80 km/h, random frequency due to irregularity of 63 Hz and defect depth of rail of 0.3 mm. In Figure 6.19, the vibration amplitude of velocity in horizontal is litter larger than that in vertical. It can be seen apparently in Figure 6.20 that the total vibration velocity at B located above the right tunnel center line on the ground surface is largest as compared with other points at further distances from the tunnel position. The results match well with reports in literature. Thus, it is known that the vibration amplitude is reduced during their propagation through the ground because of geometric and material damping (Taniguchi et al., 1997; Dong-soo et al., 2000). Figure 6.21 reveals relationship between vibration level and elapsed time of loading at B, E, H, respectively. It can be found from this result that the level tends to increases from beginning to third second during the loading and then decreases until sixth second which is the time of ending the loading.

The attenuation of vibration with distance can be also seen clearly from the results shown in Figure 6.22 and 6.23 which depict relationship between distance and maximum vibration velocity and level at Km0+940 and Km6+700 with train velocity of 80 km/h, respectively. The level of vibration rapidly decreases with distance away from the right tunnel center line for Km0+940 and the tunnel center line for Km6+700. For example at distance of 80 m from B to I and 87 m from A to I, vibration have decreased by 12 and 14 VdB at Km0+940 and Km6+700, respectively. Also, the results indicate

that regardless of the frequency of irregularity, the vibration level at the points on the ground surface of Km0+940 is higher than that of Km6+700. This is due to the tunnel at Km0+940 buried shallower. It means that the vibration has been more damped as they propagate inside soil body with larger distance from the tunnel to ground surface. However, except points of I to J at Km6+700 at a far distance of 87 to 107 m respectively from the tunnel center line for the frequencies of irregularity of 8 Hz, 16 Hz and 31.5 Hz, most points have a larger vibration level than the maximum permissible one of 75 VdB. Therefore, based on the numerical analysis results, the vibration level caused by the metro line No.3 at the two positions needs to be mitigated by the effective and appropriate measures so that it should be lower than the allowable vibration of 75 VdB. It can be seen apparently in Figure 6.23 that the maximum vibration velocity at all points of both positions is less than 5 mm/s. According to suggestion of FTA (2006) and based on consideration of current situation of nearby buildings along the line, the maximum permissible vibration velocity is accepted to be 0.2÷0.3 in/s (5.08÷7.62 mm/s). Thus, the range of vibrations that disturb the human are much less than the range that cause disturbance to the regular building. Therefore, impact of the vibration velocity on the structural buildings can be neglected.

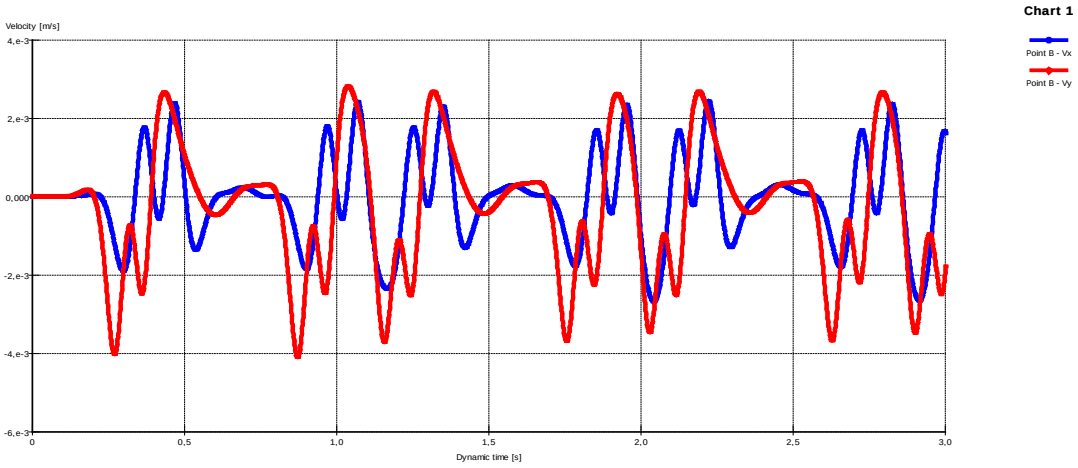


Figure 6.19 Graph of vertical and horizontal vibration velocities with time at B of Km0+940 with v = 80 km/h, f_{ir} = 63 Hz

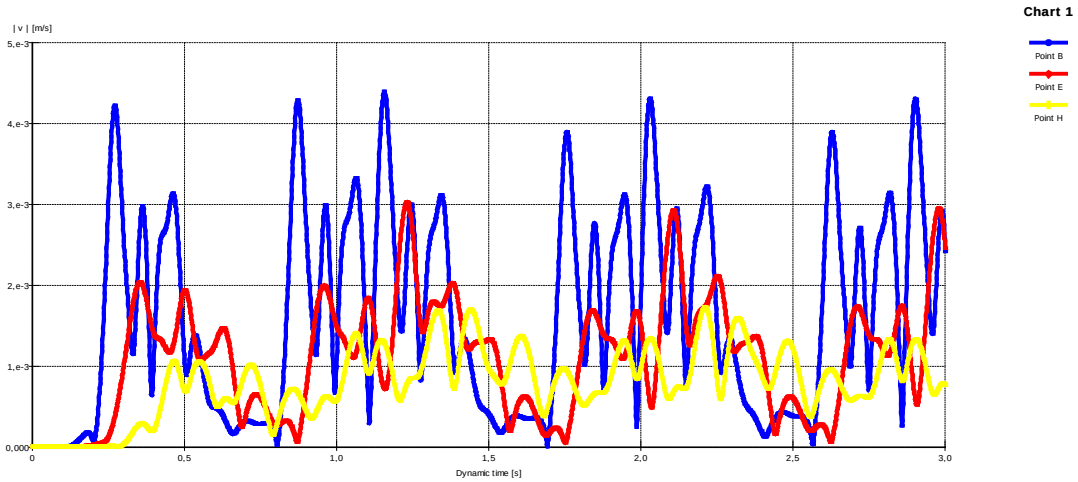


Figure 6.20 Graph of total vibration velocities with time at B, E, H of Km0+940 with v = 80 km/h, f_{ir} = 63 Hz

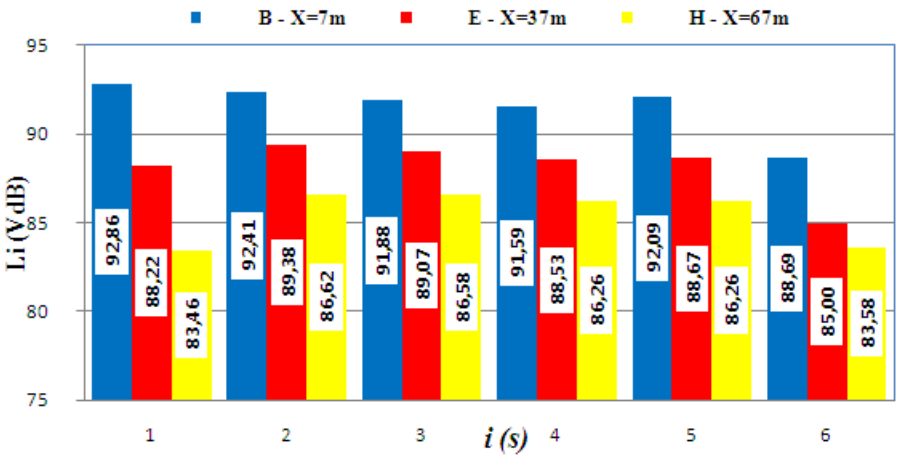


Figure 6.21 Relationship between vibration level and elapsed time of loading at B, E, H of Km0+940 with v = 80 km/h, f_{ir} = 63 Hz

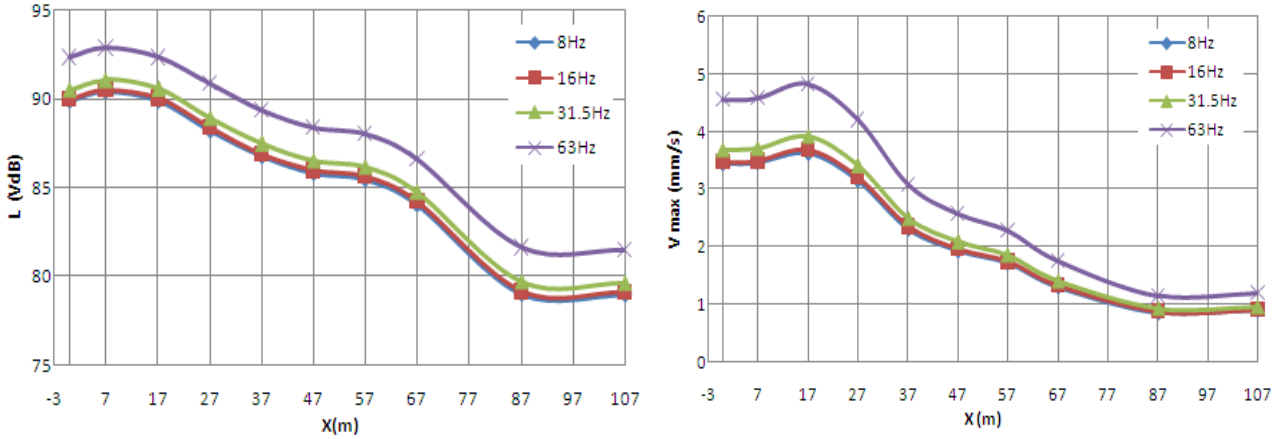


Figure 6.22 Relationship between distance and maximum vibration velocity and level at Km0+940 with v = 80 km/h

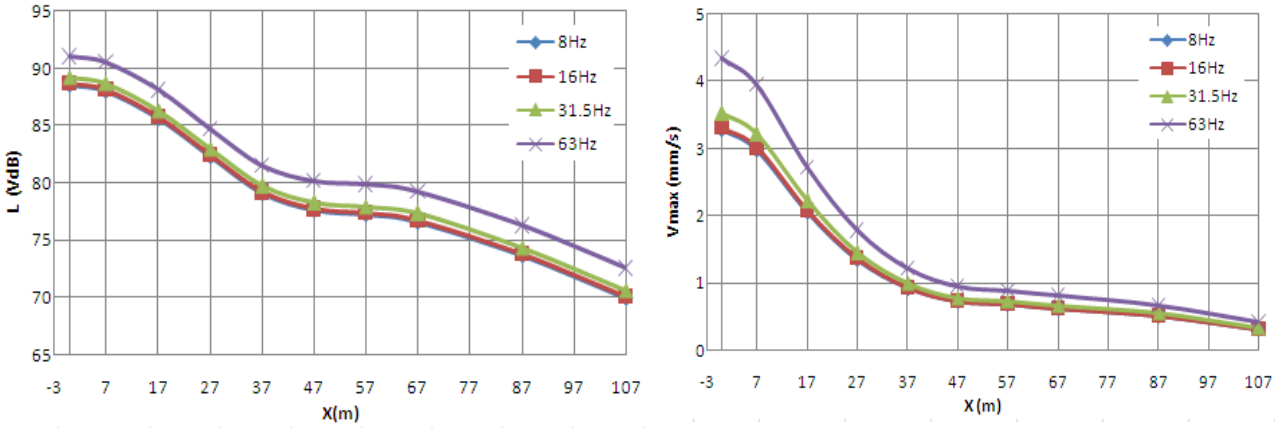


Figure 6.23 Relationship between distance and maximum vibration velocity and level at Km6+700, v = 80 km/h

6.3.3.2 Influence of random frequency due to irregularities on vibration level

Figure 6.24 shows relationship between the maximum vibration level and velocity and the random frequency at B of Km0+940 with rail defect depth, a_{ir} = 0.3 mm and train velocity, v = 80 Km/h. From the Figure, it can be realized that the vibration level increases from 0 to 2.5 VdB as the frequency increases from 8 Hz to 63 Hz corresponded with wavelength caused by the irregularity from 2.8 to 0.35 m. Therefore, before construction of the metro line, it is necessary to have a plan for maintenance of wheel and rail surface in order to avoid the arisen irregularities during operation.

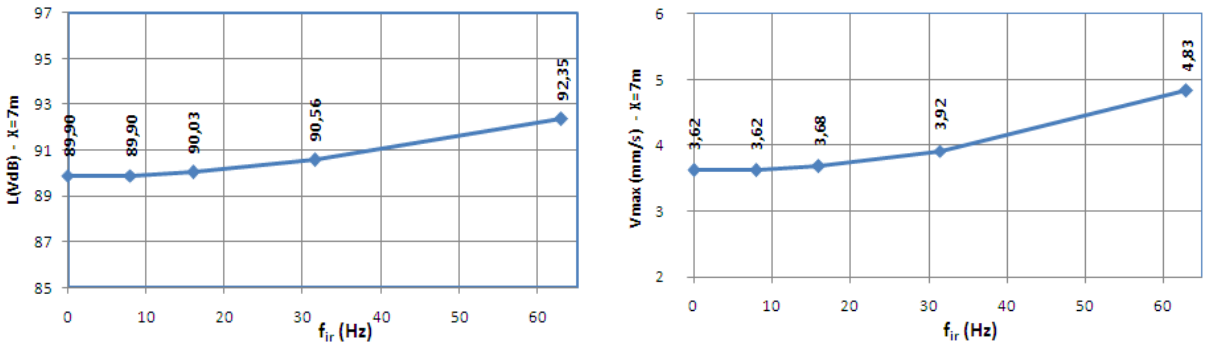


Figure 6.24 Relationship between maximum vibration level and velocity and random frequency at B of Km0+940 with v = 80 Km/h

6.3.3.3 Influence of train velocity on the vibration level

In order to evaluate the effect of train velocity on vibration, train dynamic load related to velocity of 20, 40, 60, 80 and 100 km/h was applied to the model. Figure 6.25 depicts relationship between maximum vibration level and velocity and train velocity at B of Km0+940 with the wavelength of regularity, a_{ir}=30 cm. From the Figure, it is revealed that the vibration level tends to decrease slightly as reducing the train velocity namely around 2.2 VdB per each 20 Km/h down of the velocity. The result is consistent with experiments performed by US Department of Transportation which the ground vibration increases by about 4 to 6 VdB as train speed becomes twice (Degrande et al., 2006a, b). Thus, assuming allowable vibration of 75 VdB for residence and 30 to 70 passage of train each day, as designed the velocity of train of 80 km/h, the appropriate measures should be taken to mitigate the vibrations for this metro line.

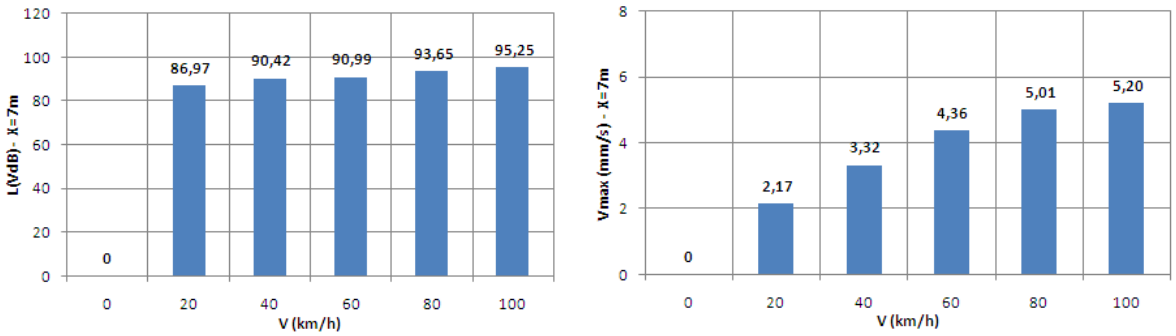


Figure 6.25 Relationship between maximum vibration level and velocity and train velocity at B of Km0+940, L_{ir} = 30 cm

6.3.3.4 Influence of tunnel shape on the vibration level

Figure 6.26 shows relationship between distance and maximum vibration velocity and level at Km6+700 in the cases of the circle and rectangle tunnel shape, respectively. The cross section geometry of the tunnels is show in Table 6.2. It can be seen from the Figure that the vibration caused by the moving train in both case circle and rectangle tunnel shape have an approximate equal level. Thus, the influence of tunnel shape on the vibration level can be neglected.

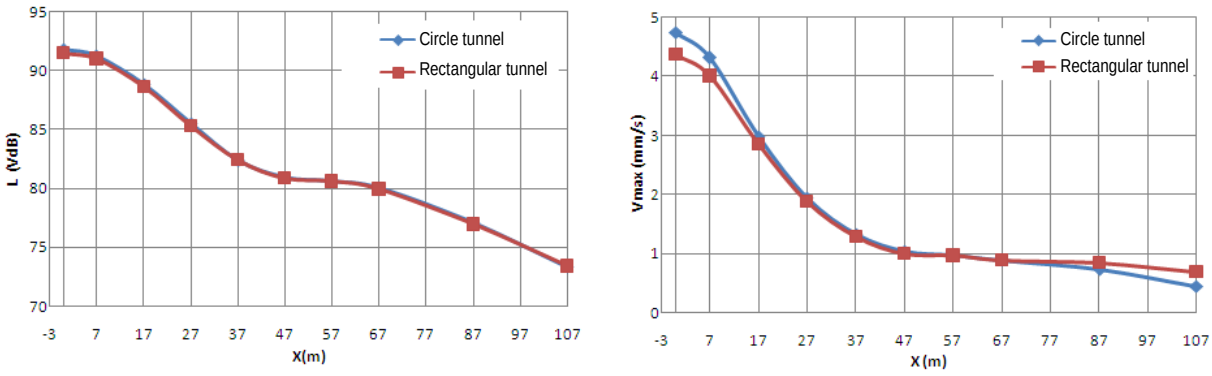


Figure 6.26 Relationship between distance and maximum vibration level and velocity at Km6+700 with v = 80 Km/h, L_{ir} = 30 cm in case of the circle and rectangle tunnel shape

6.3.3.5 Influence of sidewall thickness on the vibration level

Figure 6.27 depicts relationship between distance and maximum vibration velocity and level at Km0+940 in the cases of different sidewall thickness (20, 30, 40, 50 cm), respectively. The cross section geometry of the tunnel is show in Table 6.2. The results indicate that the vibration level is not considerably changed with decrease/increase of sidewall thickness of tunnel. Thus, the influence of the thickness on the vibration level can be neglected.

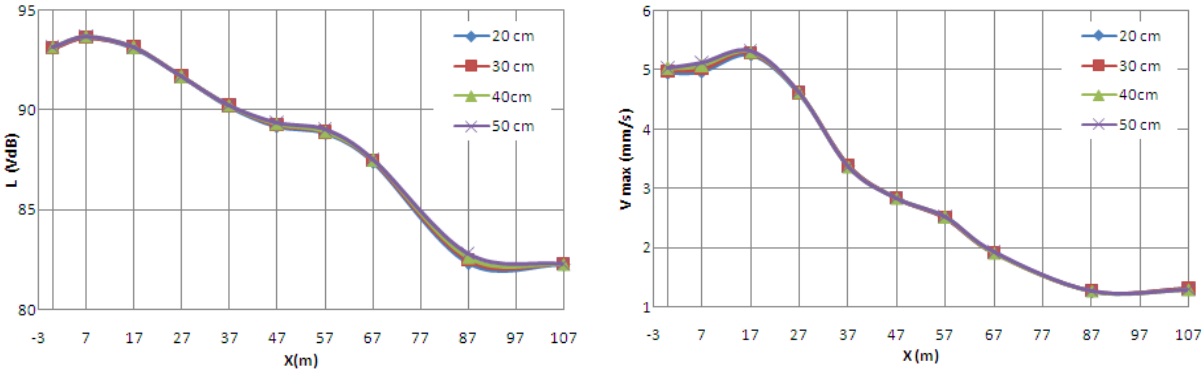


Figure 6.27 Relationship between distance and maximum vibration level and velocity at Km0+940 with v = 80 Km/h, L_{ir} = 30 cm in the case of different tunnel thicknesses

6.3.3.6 Influence of weak soil layer on the propagation of vibration velocity.

Figure 6.28 and 6.29 show the graph of vertical and horizontal vibration velocity, respectively at bottom (X = 7, Y = -16.4 m) and top (X = 7 m, Y = -4.79 m) of soil layer 1 of Km6+700. It can be seen from the Figure 6.28 that the horizontal vibration amplitude at the top is lower than that at the bottom, whereas the vertical one at the top is slightly higher as shown in Figure 6.29. As above mentioned, the layer 1 is a very weak one with thickness at this position of 9.4 m, void ratio of 2.07, degree of saturation of 97.5%, shear wave velocity of 103.01 m/s. Moreover, this layer is under water table with state of very soft to liquid. It is well known that one of wave kinds generated by train-induced vibration traveling inside soil body is the shear wave (Sinan, 2000) which hardly propagates inside liquid medium. Therefore, as a result the horizontal vibration amplitude is reduced during its propagation through the layer 1. This is consistent with a report on solution of mitigating the effect due to vibration at

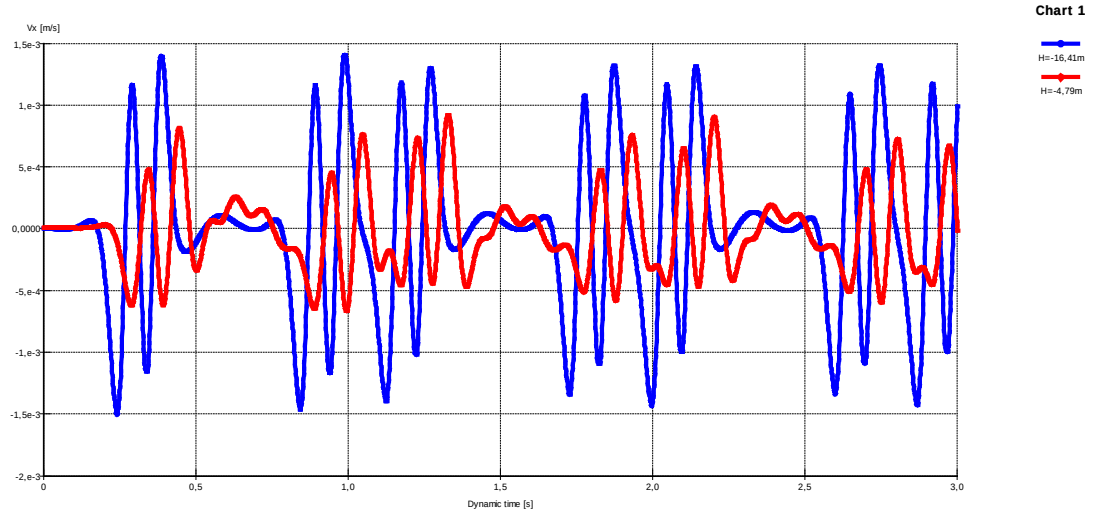


Figure 6.28 Graph of horizontal vibration velocity with time at bottom (X = 7, Y = -16.4 m) and top (X = 7 m, Y = -4.79 m) of layer 1 with v = 80 km/h, f_{ir} = 63 Hz

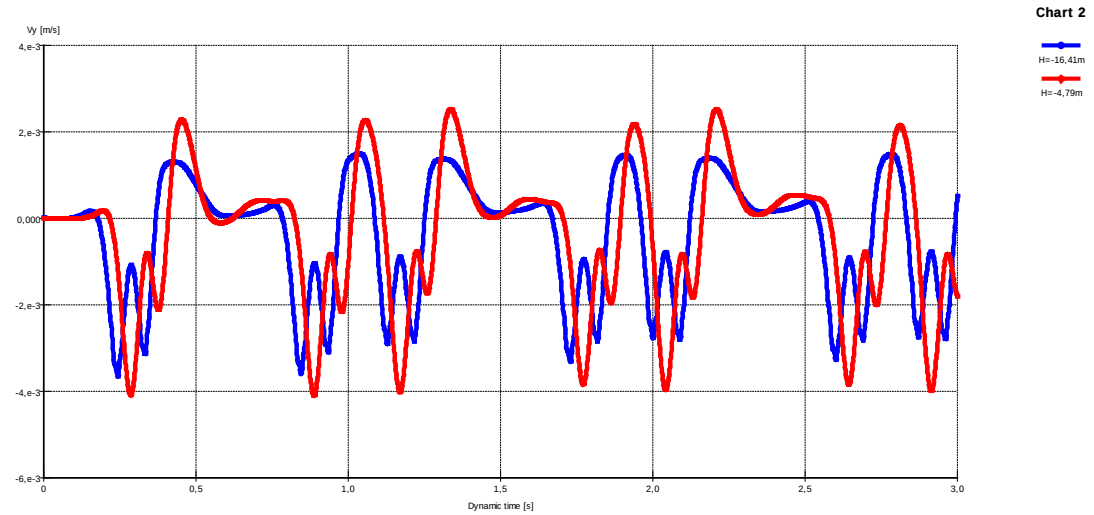


Figure 6.29 Graph of vertical vibration velocity with time at bottom (X = 7, Y = -16.4 m) and top (X = 7 m, Y = -4.79 m) of layer 1 with v = 80 km/h, f_{ir} = 63 Hz

Haiduong pottery factory in Vietnam (1972). This is also can be observed clearly in Figure 6.30 which shows the change of vibration level with depth at the position of X=7m of Km0+940 and Km6+700. Thus, the vibration level start to increase from the top of tunnel, after passing layer 1, it reduces and then, increases until reaching the surface of ground at Km6+700. Meanwhile, at Km0+940 the vibration starts its increases from the top of tunnel until the ground surface without decreases. One of the noticeable points is that the layer 1 has a much larger void ratio as compared with other layers. Moreover, experience with ground-borne vibration indicates that vibration propagation is more efficient in stiff clay soils (FTA, 2006). Accordingly, it seems that the train-induced vibration may be reduced as propagated inside soil layer which has larger void ratio than a certain value.

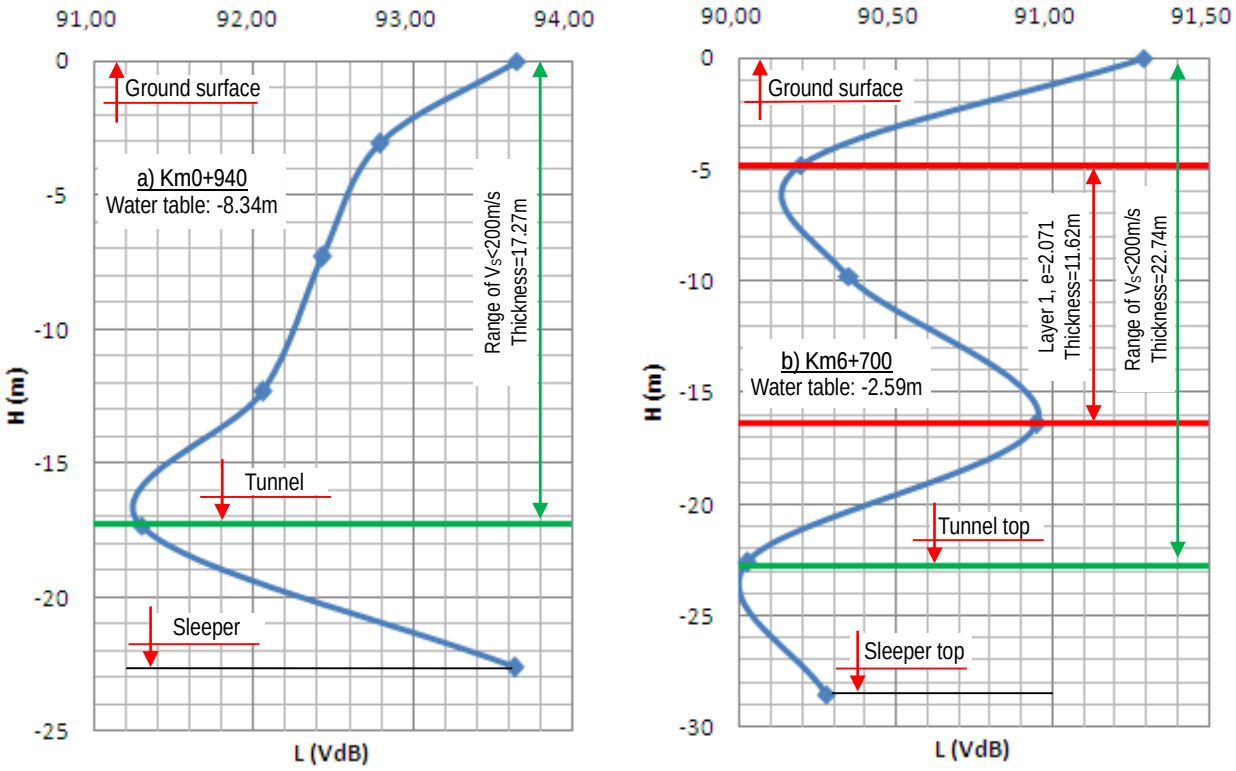


Figure 6.30 Change of vibration level with depth at X = 7 m with v = 80 km/h, L_{ir} = 30 cm

6.4 SUMMARY

Within this chapter, an analysis procedure for prediction of train-induced vibration from tunnel has been performed in conformity with current condition of Vietnam. Two cases study of tunnel shape and ground profiles, which are typical ones of Hanoi metro line No.3 currently under construction, were selected to analyze for this study. According to results of the numerical analysis, the following conclusions are reached in regard to subway induced vibrations in Vietnam.

Based on Bernoulli-Euler beam theory, a model of the dynamic loading on tunnel has been made. Its numerical simulation procedure was accomplished in Mathcad by programming. The numerical result with high reliability can be input data for ground-borne vibration analysis model.

Use of Plaxis a program being popular in Vietnam with application of Fourier spectrum method to estimate natural frequency for dynamic problem of multilayered ground system bring the reliable results

By numerical modeling in Plaxis, the vibration prediction has been performed based on the simulation. It indicated that if assuming allowable vibration of 75 VdB for residence and 30 to 70 passage of train each day, with the train velocity of 80 km/h, the vibration level at ground surface become more than 75 VdB. Thus, the appropriate measure should be taken to mitigation the vibration for the metro line No.3 in Hanoi.

REFERENCES

FTA (2006): Transit noise and vibration impact assessment, *Office of planning and environment* – Federal Transit Administration.

SP 23-105 (2004): Estimation of vibration in design, construction and operation of underground, *Code of practice for design and construction* (in Russian).

Kurbatskii, G. H. (2008): Measurement of vibrations, *Moscow State University of Railway Engineering* (in Russian).

QCVN 27:2010/BTNMT (2010): National Technical Regulation on Vibration, *Natural Resources and Environment of Vietnam* (in Vietnamese).

Tokita, Y. (1975): Vibration Pollution Problems in Japan, *In Inter-Noise 75, Sendai, Japan,* pp.465-472.

Fadeev, A. B. (1995): Finite element method in geotechnical engineering, *Education Publishing House* (translated in Vietnamese)

Bathe, K. J. (1982): Finite element procedures in engineering analysis, *Prentice-Hall Inc, Englewood Cliff, New Jersey, USA.*

Zienkiewicz, O. C. and Taylor, R. L. (2000): The finite element method, Vol.1: The basic, Butterworth-Heinemann, *A division of reed education and professional publishing Ltd.*

Zienkiewicz, O. C. and Taylor, R. L. (2000): The finite element method, Vol.2: Solid mechanics, Butterworth-Heinemann, *A division of reed education and professional publishing Ltd.*

Nguyen, T. L. (2005): Study on interaction of nonlinearity dynamic in structure and ground, *PhD. Dissertation, Le Quy Don Technical University of Hanoi* (in Vietnamese).

Nguyen, T. T. (2005): Study on interaction in structure and medium under loading of weapons with consideration of nonlinearity of medium, *PhD. Dissertation, Le Quy Don Technical University* of *Hanoi* (in Vietnamese).

Bathe K. J. and Wilson, E. L. (1973): Stability and accuracy analysis of direct integration methods, *International Earthquake Engineering and Structure*.

Brinkgreve, R. B. J. and Broere, W. (2006): *Plaxis manual version 8, Delft University of Technology* and Plaxis B. V., *The Netherlands*.

Ahmad, J. B. (2010): The modeling of lateral movement ò soft soil using finite element analysis and laboratory model, *UniTM, Shah Alma*.

Bahatin, G.(2008): Analysis of settlements of test embankments during 50 years - A comparison between field measurements and numerical analysis, *Master's Dissertation, Lund University, Sweden*.

Bui, T. S. and Nguyen, T. D. (2007): Long time stability of saturated soil under building on backfill ground in Hochiminh city and Cuulong river delta area based on Cam-Clay model, *Geotechnical Journal*, Vol.1 (in Vietnamese).

Kojic, M. and Bathe, K. J. (2005): Inelastic Analysis of Solids and Structures, *Springer-Verlag Berlin Heidenberg 2005*, Printed in Germany.

Sam, H. (2007): Applied soil mechanics with ABAQUS applications, *John Wiley & Sons, Inc., Hoboken, New Jersey.*

Hussein, M. F. M., Gupta, S., Hunt, H. E. M., Degrande, G. and Talbot J. P. (2006): An efficient model for calculating vibration from a railway tunnel buried in a half-space, *The 13 international congress on sound and vibration,* Vienna, Austria.

Hussein, M. F. M. and Hunt H. E. M. (2009): A software application for calculating vibration due to moving trains in underground railway tunnels, *Noise and vibration: Emeging method -Novem*, Oxford.

Jia, Y., Liu, W., Sun, X., Weifeng, L. and Hougui, Z. H. (2008): Dynamic responses of spatial overlapping tunnels induced by passing trains, *world Tunnel Congress 2008 - Underground Facilities for Better Environment and Safety* – India, pp.1-17.

Kurbatskii, E. H. (2008): The surface of the ground vibrations arising from fluctuations in the tunnel lining, *Moscow State University of Railway Engineering* (in Russia).

Hung, H. H. and Yang, Y. B. (2000): Elastic waves in visco-elastic half-space generated by various vehicle loads, *Soil Dynamics and Earthquake Engineering 21*.

Rajib, U., Alam, U., Waiz, A. and Subhash, R. (2008): Dynamic Analysis Of Railway Vehicle-Track Interactions Due To Wheel Flat With A Pitch-Plane Vehicle Model, *Journal of Mechanical Engineering, Transaction of the Mech. Eng. Div., The Institution of Engineers, Bangladesh,* Vol.ME39, No.2.

Di, M. G. and Di, L. C. M. (2007): A model of dynamic interaction between a train vehicle and a rail track, *4th international SIIV congress – Palermo, Italia*.

Fujii, K., Takei, Y. and Tsuno, K. (2005): Propagation properties of train-induced vibrations from tunnels, *Quarterly Report of RTRI (Railway Technical Research Institute-Japan)*, Vol.46, No.3, pp.194-199.

Pakbaz, M. S, Medizadeh, R., Vafaeian, M. and Bagherinia K. (2009): Numerical prediction of subway induced vibration: case study in Iran – Ahwaz city, *Journal of applied sciences*, Vol.9 (11), pp. 2001-2005.

Chai, J. F. and Teng, T. J. (2008): Identification of Source Time Function for Train-induced Vibration of Underground Tunnels, *17th World Conference on Nondestructive Testing*, 25-28 Oct 2008, Shanghai, China.

David, M. S. (2005): Identification and development of a model of railway track dynamic behavior, *a thesis submitted for the degree of master of Engineering – Queenland University of Technology*.

Kenney, J. T. (1954): Steady-state vibrations of beam on elastic foundation for moving load, *J Appl Mech, ASME*, 21, pp.359–364.

Paolucci, R., Maffeis, A., Scandella, L., Stupazzini, M., Vanini, M. (2003): Numerical prediction of low-frequency ground vibrations induced by high-speed trains at Ledsgaard, Sweden, *Soil Dynamics and Earthquake Engineering 23 (2003),* pp.425-433.

Esveld, C. (1989): Modern Railway Track, Duisburg, Germany, *MRT-Productions*.

Krylov, V. and Ferguson, C. (1994): Generation of low frequency ground vibrations from railway trains, *Applied Acoustics 1994,* 42, pp.199-213.

Krylov, V. (1995): Generation of ground vibration by superfast trains, *Applied Acoustics 1995*, 44, pp.149±64.

Takemiya, H. (1997): Prediction of ground vibration induced by high-speed train operation, *18th Sino-Japan Technology Seminar*, Chinese Institute of Engineers, pp.1-10

Qui, Y.J., Zang, X.J. and Wei, Y. X. (2007): Influenced of train speed on dynamic characteristics of ballastess track subgrade, *Journal of Traffic and Transport Engineering*, Vol.7, No.2.

Dahlberg T. (2003): Railway track dynamics - a survey, *Solid Mechanics/IKP*, Linköping University, SE-581, 83, Linköping, Sweden.

Alias, J. (1986): Characteristic of wave formation in rails, *Rail International*, Vol.17 (11), pp.17-23.

Gupta, S., Hussein, M. F. M., Degrande, G., Hunt, H. E. M. and Clouteau, D. (2007): A comparison of two numerical models for the prediction of vibrations from underground railway traffic, *Soil and dynamic and earthquake Eng.*, 27, pp.608-624

Kramer, S. L. (1996): Geotechnical Earthquake Eng., *Prentice Hall*, New Jersey.

Arindam, D. (2011): Calibration of a PLAXIS Finite Element Dynamic Model: Effect of Domain Width and Meshing Schemes/AES, *Third Indian Young Geotechnical Engineers Conference (3IYGEC) 25 - 26 March 2011, Indian Geotechnical Society,* New Delhi.

Ciro, V., Filippo, S. M. and Emilio, B. (2010): Comparative Study on Frequency and Time Domain Analyses for Seismic Site Response, *EJGE*.

Ciro, V. and Filippo, S. M. (2010): Some aspects of seismic design methods for flexible earth retaining structures.

Ciro, V., Filippo, S. M. and Emilio, B. (2008): Remarks on site response analysis by using Plaxis dynamic module, *Plaxis Bulletin issue 23rd March 2008*.

Amorosi, A., Elia, G., Boldili, D., Sasso, M. and Lollino, P. (2007): Analysis of the seismic response by numerical calculation, *Proc. of IARG 2007 Salerno, Italy* (in Italian)

Taniguchi, E., Sawada K. (1997): Attenuation with distance of traffic-induced vibrations, *Soil and Foundations 1979,* 19(2), pp.16–28.

Dong-Soo, K., Jin-Sun, L. (2000): Propagation and attenuation characteristics of various ground vibrations, *Soil dynamic and earthquake engineering*, 19, pp.115-126.

Degrande, G., Clouteau, D., Othman, R., Arnst, M. and Chebli, H. (2006a): A numerical model for ground vibration from underground railway traffic based on a periodic finite element-boundary element formulation, *J. Sound vibration*, 293, pp.645-666.

Degrande, G., Schevelnels, M., Chatterjee, P., Van De Velde, W. and Holscher, P. (2006b): Vibration due to a test train at variable speeds in a deep bored tunnel embedded in London clay, *J. Sound vibration*, 293, pp.626-644.

Sinan, A. S. (2000): Prediction of ground vibration from railway, *SP Swedish national testing and research institute*, SP report 2000, 25.